

Dynamic stability of complex networks

Chandrakala Meena^{1,2}, Chittaranjan Hens³, Simcha Haber¹, Stefano Boccaletti⁴⁻⁶
& Baruch Barzel^{1,2,*}

1. Department of Mathematics, Bar-Ilan University, Ramat-Gan, Israel
2. Gonda Multidisciplinary Brain Research Center, Bar-Ilan University, Ramat-Gan, Israel
3. Physics and Applied Mathematics Unit, Indian Statistical Institute, Kolkata, India
4. CNR - Institute of Complex Systems, Via Madonna del Piano 10, Sesto Fiorentino I-50019, Italy
5. Unmanned Systems Research Institute, Northwestern Polytechnical University, Xi'an 710072, China
6. Moscow Institute of Physics and Technology (National Research University), 9 Institutskiy per., Dolgoprudny, Moscow Region 141701, Russian Federation

* **Correspondence:** baruchbarzel@gmail.com

In memory of Prof. Robert May

Will a large complex system be stable? This question, first posed by May in 1972, captures a long standing challenge, fueled by a seeming contradiction between theory and practice. While empirical reality answers with an astounding yes, the mathematical analysis, based on linear stability theory, seems to suggest the contrary - hence, the diversity-stability paradox. Here we settle this dichotomy, by considering the interplay between topology and dynamics. We show that this interplay leads to the emergence of non-random patterns in the system's stability matrix, leading us to relinquish the prevailing random matrix-based paradigm. Instead, we offer a new matrix ensemble, which captures the dynamic stability of real-world systems. This ensemble helps us analytically identify the relevant control parameters that predict a system's stability, exposing three broad dynamic classes: In the asymptotically unstable class, diversity, indeed, leads to instability *à la* May's paradox. However, we also expose an asymptotically stable class, the class in which most real systems reside, in which diversity not only does not prohibit, but, in fact, enhances dynamic stability. Finally, in the sensitively stable class diversity plays no role, and hence stability is driven by the system's microscopic parameters. Together, our theory uncovers the naturally emerging rules of complex system stability, helping us reconcile the paradox that has eluded us for decades.

The study of complex social, biological and technological systems, is often directed towards dramatic events, such as cascading failures¹⁻⁵ or abrupt state transitions^{3,5,6,8,10}. In reality, however, these represent the exception rather than the rule. In fact, the truly intriguing mathematical puzzle is how, despite enduring constant perturbations and local obstructions, many systems continue to sustain reliably stable dynamics¹¹⁻¹⁵. This challenge is rooted in the *diversity-stability paradox*⁷, which predicts that a sufficiently large complex system, will inevitably become unstable. What, then, are the naturally emerging organizing principles, or in May's original wording - *what are nature's devious strategies*, to achieve this ubiquitously observed dynamic stability?

Initial clues began to unveil with the mapping of empirical networks, which uncovered universally recurring topological characteristics^{4,18,19} that can potentially impact the system's dynamics²⁰.

For example, degree heterogeneity²¹, community structure² and topological symmetries^{23,24} - all naturally emerging features of real-world networks - indeed, impact the system's dynamics²⁵⁻³⁰. However, on their own, these topological features are insufficient to ensure stability^{31,32}, leaving May's mathematical challenge unresolved.

Here, we show that the desired *devious strategies* arise not just from the network *topology*, but mainly from its interplay with the system's intrinsic, often nonlinear, interaction *dynamics*. Constrained by the physical mechanisms that drive the system's interacting components, these dynamics provide the desired, naturally emerging, *design* principles that determine the system's stability. Our analysis shows that, under real-world dynamics, stability can be fully predicted from a small set of relevant parameters that capture the combined contribution of both topology *and* dynamics. Most crucially, we identify a broad class of frequently encountered mechanisms, for which a large complex system can, and, at times, even *must* be stable, therefore settling the long overdue diversity-stability debate^{33,34}.

The diversity-stability challenge

Consider a complex system of N interacting components (nodes), whose dynamic activities $\mathbf{x}(t) = (x_1(t), \dots, x_N(t))$ are driven by nonlinear pairwise interactions. The system's fixed-points capture static states, which, unperturbed, remain independent of time. The stability of these fixed-point can be examined through their response to small perturbations $\delta\mathbf{x}$, which, in the linear regime, can be approximated by

$$\frac{d\delta\mathbf{x}}{dt} = J\delta\mathbf{x} + O(\delta\mathbf{x}^2), \quad (1)$$

where J represents the system's Jacobian matrix. We express J as⁷

$$J = W - CI. \quad (2)$$

The off-diagonal elements W_{ij} , extracted from an arbitrary distribution $P(w)$, capture the direct (linear) impact of node j on node i ; often $P(w)$ is taken to be a normal distribution $\mathcal{N}(0, \sigma^2)$. Using I to represent the identity matrix, J 's diagonal terms $J_{ii} = -C$, capture the typical relaxation times of all the nodes, which are dictated by the system's specific rate parameters. Together, $P(w)$ and C define the random *matrix ensemble* from which J is extracted. We denote this ensemble by $\mathbb{E}(P(w), C)$.

The system $\mathbb{E}(P(w), C)$ is dynamically stable if J 's principle eigenvalue satisfies $\text{Re}(\lambda) < 0$. The challenge is that, according to random matrix theory, in the limit of large N we have⁷

$$\text{Re}(\lambda) \sim \sqrt{N} \left(1 - \frac{C}{\sqrt{N}} \right), \quad (3)$$

which is positive, and hence unstable, as long as $C < \sqrt{N}$. Consequently, a sufficiently large system ($N \rightarrow \infty$) becomes inevitably unstable, *i.e.* May's paradox.

The role of the network topology. A natural attempt to reconcile this paradox is by considering structural patterns in the interaction topology A_{ij} , a binary network ($A_{ij} = 0, 1$), which is typically sparse and, most often, highly heterogeneous⁴. As J is designed to capture the *direct* response between i and j , its terms J_{ij} vanish in case there is no direct i, j link. We, therefore, write the Jacobian in (2) as $J = A \otimes W - CI$, where the Hadamard product \otimes represents matrix

multiplication element by element. Hence $J_{ij} = 0$ in case there is no link between i and j , and is assigned a weight from $P(w)$ if i and j interact. This provides the Jacobian ensemble $\mathbb{E}(A_{ij}, P(w), C)$, in which one first selects the topology A_{ij} , then assign off-diagonal and diagonal weights from $P(w)$ and C (Fig. 1a,b).

In the $\mathbb{E}(A_{ij}, P(w), C)$ ensemble, the principal eigenvalue λ depends on the average nearest neighbor degree³² κ_{nn} , whose magnitude depends on the system's degree heterogeneity². For instance, in a random network with degree distribution $P(k)$ we have^{3,32} $\kappa_{\text{nn}} = \langle k^2 \rangle / \langle k \rangle$, in which the second moment $\langle k^2 \rangle$ increase with $P(k)$'s variance, and hence with A_{ij} 's heterogeneity. Most generally, for a sufficiently broad, *i.e.* fat-tailed, $P(k)$, we have²

$$\kappa_{\text{nn}} \sim N^\beta, \quad (4)$$

an asymptotic divergence with system size. As an example, consider a scale-free network, with $P(k) \sim k^{-\gamma}$ ($2 < \gamma < 3$), for which κ_{nn} follows (3.2) with $\beta = 3 - \gamma$. Under Eq. (3.2) the principal eigenvalue in the $\mathbb{E}(A_{ij}, P(w), C)$ ensemble follows³² (Fig. 1c)

$$\text{Re}(\lambda) \sim N^{\frac{\beta}{2}} \left(1 - \frac{C}{N^{\frac{\beta}{2}}} \right), \quad (5)$$

in which the square-root of (3) is replaced by the exponent $\beta/2$. The crucial point is that, once again, we observe an asymptotic behavior that prohibits stability in the limit $N \rightarrow \infty$.

These mathematical observations, now nearing their 50th anniversary, seem to suggest that complex networked systems must be limited in size in order to maintain stability. Reality, however, consistently confronts us with the contrary³³. To reconcile this incongruity, we next show that under real nonlinear dynamics the structure of J is fundamentally different from the currently considered Jacobian ensembles. This allows us to fully predict a complex system's dynamic stability, and, down the line, disentangle May's theoretical gridlock.

The role of dynamics

The common thread that binds the present treatments of the diversity stability paradox - indeed the *paradigm* - is that one can separate the role of the topology from that of the dynamics. For example, to construct J in the $\mathbb{E}(A_{ij}, P(w), C)$ ensemble, one first selects the *topology* A_{ij} , and then independently extracts the *dynamic* response terms, W_{ij} , from $P(w)$, and the relaxation rate C . Such construction overlooks the complex interplay between A_{ij} and $P(w), C$, rooted in the nonlinear mechanisms driving the interactions between the nodes. Omitting this interplay is tantamount to ignoring the role of the system's actual nonlinear dynamics. Indeed, in $\mathbb{E}(A_{ij}, P(w), C)$, if two networks share a similar topology, they will have an equally similar J (up to statistical variations), regardless of their interaction dynamics - social, biological or technological. This, of course, stands in sharp contrast with the frequently observed fact that different nonlinear mechanisms, despite being run on similar networks, may express fundamentally distinct dynamic behaviors^{1,36,37}.

Hence, to truly predict dynamic stability, we derive the mathematical link between A_{ij} and $P(w), C$, seeking the relevant ensemble from which to extract real-world Jacobian matrices.

Dynamic mechanisms (Fig. 1d). To construct realistic J matrices we must consider each system's intrinsic dynamic mechanisms. These mechanisms are inherent to the nature of the

system's interacting components: in social systems, for example, individuals interact through infection and recovery^{38–40}, in biological networks, proteins, genes and metabolites are linked through biochemical processes^{9,10,42,44}, and in ecological systems, species undergo competitive or symbiotic interactions^{12,46,47}. All these processes capture built-in dynamics, representing the *physical* mechanisms that drive all nodes/links. Most generally, these dynamic mechanisms can be described by¹

$$\frac{dx_i}{dt} = M_0(x_i(t)) + \sum_{j=1}^N A_{ij} M_1(x_i(t)) M_2(x_j(t)), \quad (6)$$

where $M_0(x)$ captures the self-dynamics of all nodes, and $M_1(x), M_2(x)$ describe their pairwise interactions. With the appropriate selection of these nonlinear functions Eq. (1.1) captures a broad range of frequently used models in social^{38,39}, biological^{9,10,12,42,44} and technological⁴⁸ systems (Fig. 1g).

The dynamic Jacobian ensemble (Fig. 1e). Extracting J from (1.1), we show in Supplementary Section 1, leads to a currently unexplored matrix ensemble, in which the weights J_{ij} are strongly intertwined with the topology A_{ij} , via

$$J_{ii} \sim -C \kappa_{nn}^\eta k_i^\mu \quad (7)$$

$$J_{ij} \sim A_{ij} k_i^\nu k_j^\rho. \quad (8)$$

In (7) and (1.4), κ_{nn} and k_i, k_j are extracted from the *topology* A_{ij} and its degree distribution $P(k)$. The four exponents, $\Omega = (\eta, \mu, \nu, \rho)$ are, on the other hand, fully determined by the *dynamics*, $M_0(x), M_1(x), M_2(x)$, as shown in **Box I**. The coefficient C , similar to the Jacobian in (2), represents the system specific rate parameters and characteristic time-scales, a parameter that can potentially be affected by external perturbation or changing environmental conditions³.

The result is a non-random Jacobian structure, whose entries, as opposed to the existing ensembles, cannot be selected independently from an arbitrary $P(w)$, or set to a constant value C . Instead (7) and (1.4) define a new ensemble $\mathbb{E}(A_{ij}, \Omega)$, which matches, for each underlying network A_{ij} , a predictable set of weights J_{ii} and J_{ij} based on the dynamic exponents Ω . Therefore, in contrast to the random matrix based treatment of $\mathbb{E}(P(w), C)$ or $\mathbb{E}(A_{ij}, P(w), C)$, that has led the discussion since May's original analysis⁷, the newly introduced $\mathbb{E}(A_{ij}, \Omega)$ captures the effect of the system-specific nonlinear dynamics. Indeed, in (7) and (1.4), identical networks may yield highly distinctive Jacobian matrices, depending on whether the interactions are, *e.g.*, social, biological or ecological, as each dynamics is characterized by its unique set of exponents Ω (Fig. 1g).

To examine this prediction we implemented the dynamics of Fig. 1g on a set of model and relevant empirical networks. This includes four dynamic models: *Social*. The susceptible-infected-susceptible (SIS) model^{38–40} for disease spreading; *Regulatory*. The Michaelis-Menten model⁹ for gene regulation; *Ecological*. Mutualistic interactions¹² in ecology; *Biochemical*. Protein-protein interactions^{10,42,44} in sub-cellular networks. Applying each model to five different model and real networks, we arrive at a total of 20 combinations of networks/dynamics as a testing ground for our predicted J -ensemble (for a detailed description of all dynamic models and networks see Supplementary Sections 2 and 4.4).

Perturbing the system around its numerically obtained fixed-points, we constructed the Jacobian

matrix J for each of our 20 systems. In Fig. 2 we find that, indeed, the diagonal and off-diagonal terms of J follow the predicted scaling of (7) and (1.4). For example, in our Social model we predict $\mu = 1$, while our Regulatory dynamics are predicted to have $\mu = 0$, both scaling relationships clearly evident in Fig. 2a and c. This means that setting all diagonal terms uniformly to $-C$, as in May’s original formulation, misses the actual patterns that arise from the nonlinear Social/Regulatory dynamics. Similarly, the off-diagonal terms are proportional to $k_i^{-1}k_j^0$ in Social (Fig. 2b) and $k_i^0k_j^{-2}$ in Regulatory (Fig. 2d), again overruling the classic construction in which the J_{ij} entries are extracted from an arbitrary $P(w)$. These scaling relationships, encapsulated within our analytically predicted Ω , are independent of A_{ij} , as indeed Fig. 2 confirms, showing recurring scaling patterns across our model (SF1, SF2, SF3) and relevant empirical (Epoch, UCOnline, PPI1 etc.) networks. Hence, Ω captures the intrinsic, and most crucially, hitherto overlooked, contribution of the nonlinear *dynamics* to the structure of J .

To further observe J in an empirical setting, we examine in Fig. 3 the stability of our empirical social, biological and ecological networks. For each network we construct J both from the random ensemble $\mathbb{E}(A_{ij}, P(w), C)$ (left) and from the dynamic ensemble $\mathbb{E}(A_{ij}, \Omega)$ (right), where we take Ω in accordance with the relevant dynamic mechanisms (Fig. 1g). We find that the two Jacobian matrices, random vs. dynamical, despite belonging to the same network, are visibly different, as the dynamic Jacobian incorporates the emergent non-random patterns predicted in (7) and (1.4). These differences directly impact the network’s dynamic stability. Indeed, in all cases we find that the random J has a positive λ (red), congruent with May’s analysis, while the dynamic J , extracted from $\mathbb{E}(A_{ij}, \Omega)$ has $\lambda < 0$ (blue). *Hence, these empirical networks, when coupled with relevant real-world dynamics, are, in fact stable.*

Together, our analysis demonstrates that: (i) actual J matrices, extracted from real nonlinear dynamics are fundamentally distinct from random matrices; (ii) contrary to the random J ensembles, real Jacobians feature scaling patterns in which topology ($P(k)$) and dynamics (Ω) are deeply intertwined; (iii) these patterns can be analytically traced to the system’s intrinsic nonlinear mechanisms ($M_0(x), M_1(x), M_2(x)$) through Eqs. (7) and (1.4). Most crucially, while the random ensembles $\mathbb{E}(P(w), C)$ and $\mathbb{E}(A_{ij}, P(w), C)$ lead to the instability paradox of Eqs. (3) and (5), as we demonstrate in Fig. 3, and show analytically below $\mathbb{E}(A_{ij}, \Omega)$ has a much richer stability profile, in which a broad family of empirically relevant dynamics are predictably stable.

Topology, dynamics and the emergence of stability

To address May’s paradox systematically we analyze the $\mathbb{E}(A_{ij}, \Omega)$ ensemble under a fat-tailed $P(k)$, as captured by Eq. (3.2). This setting allows us to observe the combined effect of dynamic nonlinearity (Ω) with one of the most ubiquitous features of real world networks, *i.e.* degree-heterogeneity⁴. In Supplementary Section 3 we show that extracting J from $\mathbb{E}(A_{ij}, \Omega)$, with a degree-heterogeneous A_{ij} , the principal eigenvalue asymptotically follows

$$\text{Re}(\lambda) \sim N^Q \left(1 - \frac{C}{N^S} \right), \quad (9)$$

where Q and S depend both on network structure, through β in (3.2), and on the nonlinear dynamics via Ω . Specifically, we show that

$$S = \beta(1 + \nu + \rho - \mu - \eta), \quad (10)$$

replacing the fixed exponents, $1/2$ in (3), under $\mathbb{E}(P(w), C)$, and $\beta/2$ in (5), under $\mathbb{E}(A_{ij}, P(w), C)$, with a variable exponent that depends on the dynamics-driven $\Omega = (\eta, \mu, \nu, \rho)$.

Equations (9) and (3.31) represent our key result. They show that, when extracted from real nonlinear dynamics of the form (1.1), the asymptotic behavior of λ is different from the one predicted in May's original formulation, *i.e.* Eqs. (3) and (5). Most importantly, (9) and (3.31) have crucial implications regarding the system's dynamic stability, distinguishing between three potential stability classes (Fig. 1f):

- **Asymptotic instability:** $S > 0$ (red). In case S in (9) is positive, we have, for sufficiently large N , $\text{Re}(\lambda) \sim N^Q > 0$. Such systems commit to the classic diversity-stability prediction, and, when large enough, become intrinsically unstable, regardless of the model parameters (C). Specifically, setting $\eta = \mu = \nu = \rho = 0$ we revert to the random matrix ensemble ($\mathbb{E}(A_{ij}, P(w), C)$), for which $S = \beta > 0$, thus recovering May's predicted instability. Hence, the diversity stability paradox is, indeed, a valid prediction, yet it represents a specific point in a broader class of potential dynamic behaviors, driven by the parameter S in (3.31).
- **Asymptotic stability:** $S < 0$ (blue). For a broad range of empirically relevant dynamics we have $S < 0$. Under these conditions, independently of C , the r.h.s. of (9) is dominated by the negative term, guaranteeing that $\text{Re}(\lambda) < 0$. Therefore, in this class, stability is not simply *enabled*, but rather, under $N \rightarrow \infty$, it becomes asymptotically inevitable, even if $C \ll 1$. Recalling May's original question: *can a large complex system be stable?* - Eq. (9) with $S < 0$ provides a clear answer: it not only *can*, but, in fact, *must* be stable.
- **Sensitive stability:** $S = 0$ (green). Under $S = 0$ the system lacks an asymptotic behavior, and therefore, its stability depends on C in (9). If $C > 1$, *i.e.* sufficiently strong negative feedback, the system is stable, otherwise it becomes unstable. As opposed to Ω , which is intrinsic to the dynamic *model*, depending on the functional form of $M_0(x), M_1(x), M_2(x)$ in (1.1), C is determined by the specific model *parameters*. Hence, in this class stability is not an intrinsic characteristic of the system, but rather it is sensitive to Eq. (1.1)'s tunable parameters.

This classification settles the debate on complex system stability on several levels. In the context of the diversity-stability paradox, it shows that large complex systems *can*, and in some cases even *must* be stable - hence reconciling between theory and empirical observation. More broadly, the stability classifier S , identifies the relevant topological (β) and dynamic (Ω) control parameters that help analytically predict the stability class of any system within the form (1.1). We can therefore use S to predict *a priori* whether a specific combination of topology and dynamics will exhibit stable functionality or not.

To examine our stability classifier S we used our model and real networks to extract 2,077 Jacobian matrices from the $\mathbb{E}(A_{ij}, \Omega)$ ensemble, with different sets of η, μ, ν and ρ . In Fig. 4a we show the principal eigenvalue λ vs. S for the entire 2,077 Jacobian sample. As predicted, we find that the parameter S sharply splits the sample into three classes. The asymptotically unstable class (red, top-right) has $S > 0$ and consequently also $\lambda > 0$, a guaranteed instability. The asymptotically stable class (blue, bottom-left) is observed for $S < 0$, and has, in all cases $\lambda < 0$, *i.e.* stable dynamics, as predicted. Finally, for $S = 0$ we observe sensitive stability, with λ having no asymptotic positive/negative assignment (green). A small fraction ($\sim 4\%$) of our sampled J matrices were inaccurately classified by S (grey), a consequence of the approximate nature of our derivations (Supplementary Section 3).

In Fig. 4a we also present the stability matrices associated with our empirical social, biological and ecological networks (symbols) examined earlier in Figs. 2 and 3. For each of these networks we constructed J via the $\mathbb{E}(A_{ij}, P(w), C)$ ensemble, assigning random weights along the links, as well as via the $\mathbb{E}(A_{ij}, \Omega)$ ensemble, with weights determined by (7) and (1.4), and Ω taken according to the relevant dynamic model (Fig. 1g). While all these networks are classified unstable under the random ensemble (red symbols), as per May’s diversity-stability principle, once fit with J from our dynamic ensemble they all transition into the asymptotically stable class (blue symbols).

Figures 2 - 4, together demonstrate our complete theoretical path: First, Figs. 2 and 3 show that real J matrices exhibit the internal scaling patterns predicted in (7) and (1.4) - representing a steep departure from the broadly applied random matrix paradigm. Next, Fig. 4 shows that the resulting Jacobian ensemble has a rich space of potential dynamic behaviors, significantly more diverse than the currently considered ensembles. Most importantly - this space contains a broad class of asymptotically stable (blue) or sensitively stable (green) systems, that do not fall within May’s paradox.

Taken together, our analysis demonstrates that nature must not rely on devious strategies in order to ensure dynamic stability. The observed stability of large complex systems emerges quite naturally thanks to the built-in nonlinear interaction mechanisms between the system’s components.

The ingredients of dynamic stability

The parameter S in (3.31) reduces a network’s dynamic stability into five relevant exponents. The first four $\Omega = (\eta, \mu, \nu, \rho)$ are determined by the nonlinear dynamics, Social, Regulatory, Ecological etc., and are therefore intrinsic to the system’s inherent interaction mechanisms. These exponents are independent of the topology A_{ij} or of the microscopic model parameters, all of which are encapsulated within C . Therefore they are *hardwired* into the system’s dynamic behavior. To understand this, consider, for example, our Social model, for which our formalism predicts $\Omega = (0, 1, -1, 0)$. This prediction is rooted in the SIS interaction mechanisms, *i.e.* infection vs. recovery, expressed through the functional form of $M_0(x), M_1(x), M_2(x)$ of (1.1). It is, therefore, insensitive to the specific parameters of the model, *e.g.*, if the disease has a high or low infection rate, or if it is transmitted via physical contact or aerosols. Such distinctions, expressed through the model *parameters*, may impact the coefficient C , but do not affect Ω , and therefore have no bearing on the stability classifier S . Hence, S is characteristic of, *e.g.*, the SIS *model*, not of its specific *parameters*.

The remaining exponent in (3.31), β , is independent of the dynamics, determined solely by A_{ij} , specifically by its degree distribution $P(k)$, through (3.2). This parameter quantifies the fat-tailed nature of $P(k)$, being $\beta = 0$ for a bounded distribution, and approaching unity under extreme levels of degree-heterogeneity. Therefore, together, S captures the roles of both topology *and* dynamics, whose interplay determines the system’s stability class - stable, unstable or sensitive.

The role of degree-heterogeneity. The prevalence of fat-tailed $P(k)$ is among the defining features of real-world complex systems, from biological⁴⁹ to social^{16,17} and technological^{52,53} networks, with far-reaching implications on their observed dynamic behavior^{1,3,32}. Our analysis indicates that this network characteristic may also play a crucial role in the context of dynamic stability. To understand this, consider a non fat-tailed $P(k)$, such as an Erdős-Rényi, network,

where the degrees follow a Poisson distribution, having $\beta = 0$. Under these conditions we have $S = 0$ in (3.31), the system has no defined asymptotic behavior, and hence it is sensitively stable - *i.e.* its stability depends on model parameters. Therefore, the existence of asymptotic stability/instability is a direct consequence of degree-heterogeneity, as, indeed, these forms of dynamic stability rely on $\beta > 0$.

This uncovers a new additional layer to the dynamic impact of $P(k)$ on complex system functionality. Consider, for example, the factors that drive a system towards the loss of stability. Most often such events result from external stress or changes in environmental conditions³. Such forces impact a system's functionality by perturbing its dynamic parameters, namely they affect the coefficient C . Seldom, however, do these environmental perturbations affect the system's built-in interaction mechanisms. Indeed, while the dynamic mechanisms are fixed, ingrained in the *physics* of the interacting components, the specific model parameters often depend on external conditions. The crucial point is, that under $S < 0$, a state only possible if $P(k)$ is fat-tailed (*i.e.* $\beta \neq 0$), stability becomes asymptotically independent on C , driven solely by Ω , which is insensitive to specific model parameters. Hence, for a sufficiently large system ($N \rightarrow \infty$), if $P(k)$ is fat-tailed, stability becomes asymptotically robust against any external perturbation. *This suggests that degree-heterogeneity serves as a dynamically stabilizing topological characteristic, in the face of a persistently fluctuating environment.*

To illustrate this, consider again the SIS model (Social), for which $\Omega = (0, 1, -1, 0)$, and hence Eq. (3.31) predicts $S = -\beta$. Implemented on a scale-free network ($\beta > 0$), Social has $S < 0$, and is thus asymptotically stable. However, the same dynamics on a bounded $P(k)$ ($\beta = 0$) becomes sensitively stable, *i.e.* $S = 0$, and therefore its stability depends on the specific value of C , which can be tuned by changing the infection/recovery rates. Consequently, while generally Social's pandemic state is only stable if C in (9) is greater than unity, in a scale-free environment it is *always* stable, even when $C \rightarrow 0$. This observation, predicted here directly from our formalism, recovers an already well-established result: the fact that in the SIS model, the epidemic threshold vanishes under a scale-free $P(k)$ ⁵⁴. The crucial point is, however, that while the original result, particular to the SIS model, was obtained using a dedicated model-specific analysis, our control parameter S allows us to systematically analyze the stability profile of *all* combinations of topology/dynamics within (1.1), using a single universal classification.

To observe this role of $P(k)$, beyond the specific example of Social, we consider again $\mathbb{E}(A_{ij}, \Omega)$'s principal eigenvalue λ in (9). Its structure portrays stability as a balance between the positive, *i.e.* destabilizing, effect mediated by the network interactions, vs. the negative, stabilizing, feedback, driven by the parameter C in J 's diagonal (7); Fig. 4b. It is therefore, natural to enhance stability by increasing C , which, in effect, translates to strengthening each node's intrinsic negative feedback. Equation (9) predicts that a system becomes stable if C exceeds a critical value

$$C_0 \sim N^S, \tag{11}$$

beyond which λ becomes negative. For asymptotically stable systems ($S < 0$) we have $C_0 \rightarrow 0$, a guaranteed stability even under arbitrarily small C . In contrast, for asymptotically unstable systems ($S > 0$) we have $C_0 \rightarrow \infty$, hence such systems are impossible to stabilize even under extremely large C , *i.e.* extreme levels of negative feedback. The point is, that if $P(k)$ is bounded we have, always, $S = 0$ (sensitive stability), hence C_0 is finite, and the system's stability can be controlled by tuning the parameter C , *e.g.*, changing the environmental conditions.

In Fig. 4c-k we extract again a set of three J matrices from $\mathbb{E}(A_{ij}, \Omega)$, representing systems from our three stability classes: J_{AS} , asymptotically stable with $\Omega = (2, 2, 2, -1)$; J_{SS} , sensitively stable with $\Omega = (0, -1, -2, 0)$; and J_{AU} , asymptotically unstable with $\Omega = (1, -2, -1, 2)$. For each of these we plot C_0 vs. N , capturing the level of negative feedback required to ensure the system's stability. Under an Erdős-Rényi network, with bounded $P(k)$ ($\beta = 0$) we do not observe a defined asymptotic behavior. The critical C_0 does not scale with N , indicating that sufficient perturbation to the model parameters can affect the system's stability (Fig. 4i-k, green circles).

The picture, however, fundamentally changes when we construct the same J matrices from a scale-free A_{ij} with $\beta = 0.6$ (Fig. 4f-h, squares). Now we have $S = -1.2, 0$ and 1.8 for J_{AS}, J_{SS} and J_{AU} , respectively. As predicted in (11), under these condition, we observe a clear asymptotic behavior, in which C_0 scales with N . For J_{AS} we have $C_0 \sim N^{-1.2}$, while under J_{AU} we observe $C_0 \sim N^{1.8}$ (solid lines), capturing the intrinsic stability/instability of these two systems. Finally, in J_{SS} , having $S = 0$, the system does not feature any asymptotic behavior, and therefore can be stabilized under finite C_0 , independently of system size N (Fig. 4g).

Hence, we observe a qualitative difference between bounded vs. scale-free $P(k)$, in which degree heterogeneity can potentially afford the network a guaranteed stability, that is asymptotically independent of microscopic parameters.

Stabilizing vs. destabilizing dynamics. To gain qualitative insight on the role of the non-linear dynamics, beyond the formal prediction of Eq. (3.31), let us focus on a specific test case of Ecological interactions, in which Eq. (1.1) takes the form (Fig. 1g)

$$\frac{dx_i}{dt} = Bx_i(t) \left(1 - \frac{x_i(t)}{K} \right) + \sum_{j=1}^N A_{ij}x_j(t)F(x_j(t)). \quad (12)$$

The self-dynamics follows logistic growth⁵⁵ and the interaction mechanism describes mutualistic dynamics¹². The response function $F(x_j)$ is designed to capture the positive contribution of node j 's activity to that of node i . Often this contribution is taken to follow $F(x_j) = x_j$, assuming a linear contribution of a species' abundance to its symbiotic partners. Such dynamics lead to $\Omega = (0, 1, 1, 0)$, which in (3.31) provides $S = \beta > 0$, predicting an asymptotically unstable dynamics. The source of this instability is rooted in the strong positive feedback between interacting nodes, in which an increase in x_j is linearly transferred to x_i 's growth rate.

An alternative formulation, which we used in our simulations in Fig. 2e,f, takes $F(x_j) = x_j/(1+x_j)$. This represents a saturating function, in which j 's impact on i is bounded, as, indeed, in the limit $x_j \rightarrow \infty$ we have $F(x_j) \rightarrow 1$. Under this response function, the exponent ρ changes from $\rho = 0$, observed in the linear $F(x_j)$, to $\rho = -2$, under the saturating alternative. Consequently, we now have $\Omega = (0, 1, 1, -2)$, predicting $S = -\beta$, and therefore, the same network which was unstable under $F(x_j) = x_j$ is now asymptotically stable thanks to $F(x_j)$'s saturation.

From an intuitive perspective, as $F(x_j)$ becomes bounded, the interaction is *weakened*. This is expressed formally in (1.4) through the suppressed off-diagonal terms J_{ij} , here - due to the negative exponent $\rho = -2$. This reduction in J_{ij} , in turn, leads to a diminished λ . In that sense, the stability classifier S in (3.31) captures precisely this balance: if ν, ρ are large - the off-diagonal terms J_{ij} , which represent positive feedback, dominate the system's dynamics, S becomes positive and the system is asymptotically unstable. Conversely, if μ, η are increased, the diagonal terms in (7) carry sufficient weight to asymptotically stabilize the system. The case

$S = 0$ captures a balance between J_{ii} and J_{ij} , rendering the system sensitive to its microscopic parameters. Hence, despite their formal mathematical nature (*Box I*), the four exponents η, μ, ν and ρ provide qualitative insight into the dynamic ingredients that govern the network's stability (Fig. 5).

Levels of dynamic stability. While stability is, in its essence, a binary classification - a system is either stable or not, we can use S to quantify the *level* of the system's stability. Consider again Eq. (11), capturing the critical value of C in (7) required to stabilize the system's dynamics. An asymptotically stable system has $C_0 \rightarrow 0$, *i.e.* stability is ensured even under arbitrarily small C . In contrast, an asymptotically unstable system has $C_0 \rightarrow \infty$, hence cannot be stabilized under finite parameters. These effects are pronounced more strongly as S becomes more negative (stable) or more positive (unstable). As an example, let us compare Regulatory dynamics with $h = 1, a = 2$, under which we have $S = -\beta/2$, vs. Ecological dynamics, where $S = -\beta$. Both are asymptotically stable, yet Eq. (11) indicates that Ecological is *more* stable: to destabilize Ecological one needs $C_0^{\text{Eco}} \sim N^{-\beta}$, while for Regulatory it is sufficient to have $C_0^{\text{Reg}} \sim N^{-\beta/2}$, hence $C_0^{\text{Eco}} \ll C_0^{\text{Reg}}$. The meaning is that to destabilize Ecological we much reach a more extreme reduction in C than the one required for Regulatory. In Fig. 5b we show the lines of equi-stability, comprising all dynamics with the same S value, and hence a similar level of stability/instability. These equi-stable classes may group together highly distinct dynamics, that despite their different Ω may have identical S . For example, Social and Ecological, two dynamics from fundamentally different domains, that exhibit a similar level of stability, belonging to the class $S = -\beta$ (Fig. 1g).

Mixed interactions. Our analysis up to this point focused on cooperative mechanisms, in which $M_1(x)$ and $M_2(x)$ are positive, as observed, *e.g.*, in mutualistic ecological dynamics^{3,28}. To complement this, in Supplementary Section 5 we numerically analyze the case of mixed dynamics, in which a fraction f of positive interactions coexists alongside a $1 - f$ fraction of negative ones. We find that for a broad range of f values, our predicted asymptotic stability continues to be observed. This is attributed, once again, to a naturally emerging organizing principle, relevant in many real-world systems: the fact that the activities $x_i(t)$ in (1.1) are, by definition, non-negative. Therefore, as the system evolves in time, at any instance where a node reaches $x_i(t) = 0$ it becomes extinct, and permanently removed from the network. This ratchet-motion prunes out nodes with many negative interacting partners, as their activities are naturally driven towards zero. As a result, the system reaches a fixed-point in which the majority of remaining links is biased towards positive interactions. Under these conditions, the emergent Jacobian matrix J_{Mix} , while still featuring some level of negative interactions, is predominantly positive. Therefore, despite the fact that, strictly speaking, $J_{\text{Mix}} \notin \mathbb{E}(A_{ij}, \Omega)$, it continues to *approximately* follow the patterns of (7) and (1.4), and most importantly in the present context - continues to allow a broad class of asymptotically stable systems.

Discussion and outlook

The linear stability matrix J carries crucial information on the dynamic behavior of a complex system. Here, we exposed distinct patterns in the structure of J that (i) arise from the nature of the system's interaction dynamics; (ii) affect its principal eigenvalue, and thus, its stability profile. These patterns are expressed through the four dynamic exponents $\Omega = (\eta, \mu, \nu, \rho)$ in (7) and (1.4), linked analytically to the system's dynamics, $M_0(x), M_1(x), M_2(x)$, through the leading powers of the expansions in Eq. (1.65). This dependence on the *powers* ($\Psi(n), \Gamma(n)$, etc.), rather than the *coefficients* (G_n, C_n , etc.) indicates that Ω is hardwired into the interaction

dynamics. Indeed, the powers in (1.65) are determined by the dynamic model, *e.g.*, Social or Regulatory, but not the specific model parameters, which only impact the coefficients. Therefore, our predicted Jacobian ensemble in (7) and (1.4), as well as its associated stability classifier S in (3.31), both capture highly robust and distinctive characteristics of the system’s dynamics, that cannot be perturbed or otherwise affected by shifting environmental conditions.

Graph spectral analysis represents a central mathematical tool to translate network structure into dynamic predictions^{56–58}. A network’s spectrum, *i.e.* its set of eigenvalues and eigenvectors, captures information on its dynamic time-scales, potential states, and - in the present context - its dynamic stability. *In that sense, the long-standing diversity-stability paradox exposed a severe and troubling clash between spectral graph theory and empirical observation. Here we reconcile this contradiction, by showing that, in effect, we have, all this time, been looking at the wrong spectrum.* Indeed, in its current application, spectral analysis is applied to the network *topology*, namely we seek the graph’s eigenvalues. Focusing on the graph topology, however, loses information on the nonlinear dynamics that occur *on* that graph. Therefore, here, we offer to apply spectral analysis, not to the topology A_{ij} , but rather to the derived Jacobian in (7) and (1.4), which, thanks to Ω preserves the information of both topology *and* dynamics.

In a broader perspective, the interplay between topology and dynamics is one of the major theoretical obstacles along the path to predict, understand and control complex system behavior^{59–62}. The problem is that we lack sufficient theoretical tools to treat the challenging combination of nonlinear dynamics with complex, random and often highly heterogeneous network structures. Consequently, advances are often system specific, requiring dedicated tools, and hence, lacking the breadth of a general network dynamics theory. The Jacobian ensemble presented here, transforms the nonlinear Eq. (1.1) into an effective linear system, whose weights depend on both topology and dynamics. It can, therefore, allow us to utilize the powerful tools of spectral graph theory, even in a nonlinear dynamic setting. This may offer a basis for systematic analysis of nonlinear network dynamics.

Data availability. Upon acceptance, all codes/data to reproduce our analysis will be made available online.

BOX I. THE ENSEMBLE $\mathbb{E}(A_{ij}, \Omega)$ - HOW TO CALCULATE Ω

To construct J as appears in Eqs. (7) and (1.4) we must extract the exponents $\Omega = (\eta, \mu, \nu, \rho)$ from Eq. (1.1). First we use the dynamic functions $M_0(x), M_1(x)$ and $M_2(x)$ to construct three new functions

$$R(x) = -\frac{M_1(x)}{M_0(x)}, \quad Y(x) = M_1(x)R'(x), \quad Z(x) = R(x)M_2(x), \quad (13)$$

where $R'(x)$ represents a derivative dR/dx around the fixed point \mathbf{x} . From these we extract four additional functions, which we express through a Hahn power-series expansion as

$$\begin{aligned} M_2(Z^{-1}(x)) &= \sum_{n=0}^{\infty} G_n x^{\Psi(n)}, & Y(R^{-1}(x)) &= \sum_{n=0}^{\infty} C_n x^{\Gamma(n)}, \\ M_1(R^{-1}(x)) &= \sum_{n=0}^{\infty} K_n x^{\Pi(n)}, & M_2(R^{-1}(x)) &= \sum_{n=0}^{\infty} L_n x^{\Theta(n)} \end{aligned}, \quad (14)$$

where $R^{-1}(x)$ and $Z^{-1}(x)$ represent the inverse functions of $R(x)$ and $Z(x)$. The Hahn expansion⁶ is a generalization of the Taylor expansion to include negative and real powers. Hence $\Psi(n), \Gamma(n), \Pi(n)$ and $\Theta(n)$ represent series of real powers in ascending order, the leading (*i.e.* smallest) powers assigned the index $n = 0$. These leading powers directly provide Ω via

$$\mu = 2 - \Gamma(0), \quad \nu = -\Pi(0), \quad \rho = -\Theta(0), \quad \eta = -\Psi(0)(\mu - \nu - \rho). \quad (15)$$

Hence, to construct $J_{ij} \in \mathbb{E}(A_{ij}, \Omega)$ we first generate the network A_{ij} , then extract the degrees k_i of all nodes and the nearest neighbor degree κ_{nn} . The resulting J_{ij} satisfies

$$J_{ii} \sim -C \kappa_{\text{nn}}^{\eta} k_i^{\mu} \quad (16)$$

$$J_{ij} \sim A_{ij} k_i^{\nu} k_j^{\rho}, \quad (17)$$

where the constant $C > 0$ captures the system's specific dynamic time-scales. Note that Ω , as opposed to C , depends only on the leading *powers* of (1.65), and not on the *coefficients*. Therefore it is unaffected by Eq. (1.1)'s microscopic parameters, capturing an intrinsic characteristic of each dynamic model. The detailed derivation of Ω appears in Supplementary Section 1, followed by a step by step application on all our dynamic models (Fig. 1g) in Supplementary Section 2.

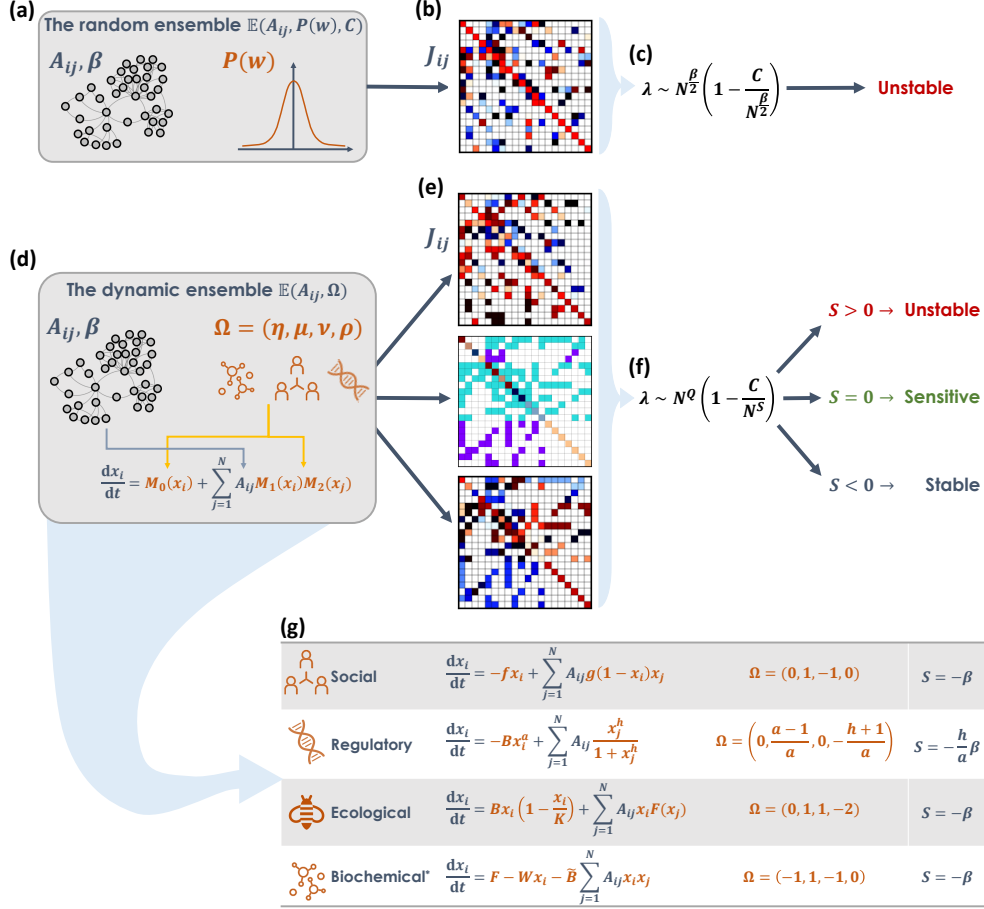


Figure 1: **Solving the diversity-stability paradox.** (a) A complex system is captured by an interaction network A_{ij} , whose diversity can be quantified by β in (3.2). In May’s random matrix framework, to assess dynamic stability, we construct the Jacobian J with weights extracted independently from the distribution $P(w)$, and diagonal term set to $-C$ (constant). (b) The resulting stability matrix J_{ij} , belonging to the ensemble $\mathbb{E}(A_{ij}, P(w), C)$. (c) The principal eigenvalue, under this construction, diverges with the number of interacting components N , predicting that a large system *cannot* be stable. This non-realistic prediction captures the unresolved diversity-stability paradox. (d) Our alternative J -ensemble, $\mathbb{E}(A_{ij}, \Omega)$, is designed to capture the roles of both the network (A_{ij}, β , grey) and the nonlinear dynamic mechanisms of interaction, *e.g.*, Biochemical, Social or Regulatory (orange). These mechanisms are described by $M_0(x), M_1(x), M_2(x)$ in Eq. (1.1), from which we extract the four exponents of Ω . Here, the diagonal and off-diagonal weights of J are not selected independently from $P(w), C$, but rather predicted by Eqs. (7) and (1.4). (e) As a result, the same A_{ij} may lead to different J matrices, as different dynamics are characterized by distinct Ω . (f) Consequently, λ follows a different form than in (c), with a variable *stability classifier* S , whose sign predicts the system’s stability: Unstable (red) in which diversity, indeed, leads to instability; Sensitive (green), where diversity plays no role, and Stable (blue), in which diversity *enhances* stability. Hence, under real nonlinear dynamics a large system *can* ($S = 0$), and in some cases even *must* ($S < 0$) be stable. (g) We use four common dynamic models capturing Social, Regulatory, Ecological and Biochemical interactions to examine our theoretical analysis. For each of these dynamics we extract Ω and S , as detailed in Supplementary Section 2. *For the calculation of S in Biochemical see Supplementary Section 3.2.

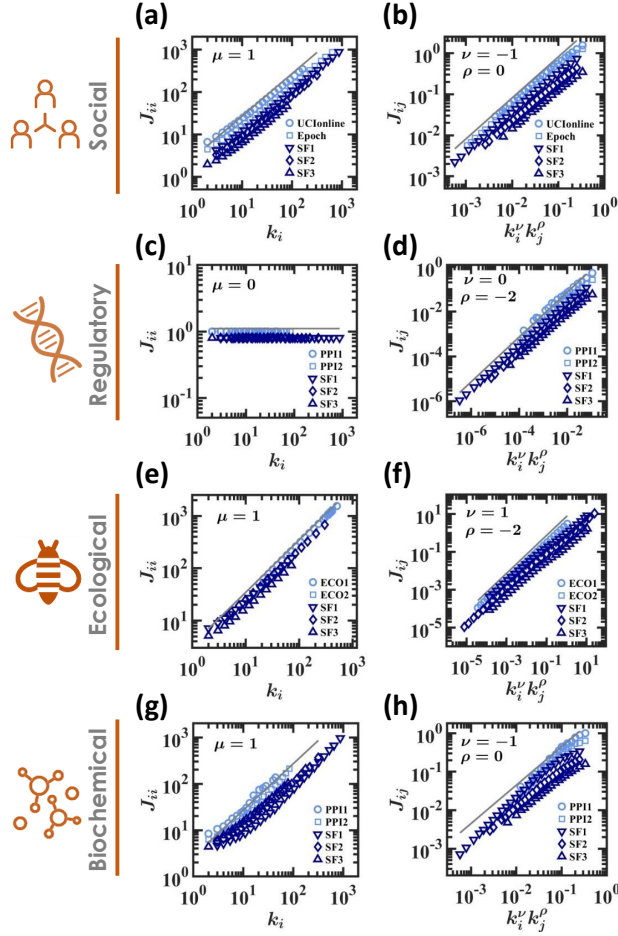


Figure 2: **Emerging patterns in the dynamic ensemble** $\mathbb{E}(A_{ij}, \Omega)$. We implemented Social, Regulatory, Ecological and Biochemical dynamics (Fig. 1g) on a set of relevant model (dark blue) and empirical (light blue) networks. Perturbing all nodes we numerically constructed each system's Jacobian, J , capturing *real* Jacobian matrices, as obtained from actual nonlinear dynamic models. (a) The diagonal terms J_{ii} vs. degree k_i as obtained from Social dynamics (symbols). We observe the scaling relationship of Eq. (7) with $\mu = 1$ (solid line) confirming our predicted scaling for this dynamics. (b) The off diagonal terms J_{ij} vs. prediction (1.4) with $\nu = -1, \rho = 0$ (symbols). Once again, we observe a perfect agreement with our theoretical prediction (solid line). We also include results obtained from two relevant empirical networks, Epoch¹⁷ and UCInonline¹⁶, capturing online social dynamics. (c) - (d) Similar results are observed under Regulatory dynamics ($\mu = \nu = 0, \rho = -2$) on both model and real networks (PPI1¹⁸ and PPI2¹⁹); (e) - (f) Ecological dynamics ($\mu = \nu = 1, \rho = -2$, empirical networks: ECO1 and ECO2²⁰); (g) - (h) Biochemical dynamics ($\mu = 1, \nu = -1, \rho = 0$, empirical networks: PPI1 and PPI2). As predicted, we find that real Jacobian matrices exhibit the non-random patterns of Eqs. (7) and (1.4), and therefore cannot be modeled via the random ensemble $\mathbb{E}(A_{ij}, P(w), C)$, but rather through our dynamic Jacobian family $\mathbb{E}(A_{ij}, \Omega)$. Data in all panels are logarithmically binned¹⁵. Details on the numerical calculation of J , log-binning and the construction of all model/real networks appear in Supplementary Section 4.

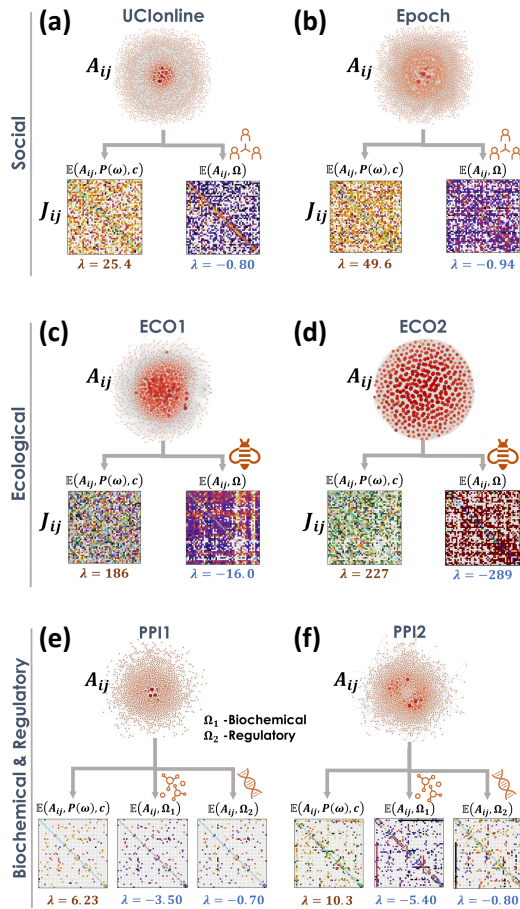


Figure 3: **The dynamic J ensemble in empirical networks.** (a) Using the real social network, UCInonline, we extracted the Jacobian J from the random ensemble $\mathbb{E}(A_{ij}, P(w), \Omega)$ (left). The resulting J matrix has $\lambda = 25.4 > 0$, and is, therefore unstable, as per May's prediction. Implementing our Social dynamics (SIS) we constructed J again, this time using our predicted $\mathbb{E}(A_{ij}, \Omega)$ (right). The resulting J is visibly different, owing to the emergent patterns of (7) and (1.4). Most importantly, it has $\lambda = -0.80 < 0$, and hence despite the random matrix prediction, the system is, in fact, stable. (b) Similar results are obtained from Epoch, with $\lambda = 49.6 > 0$ under $\mathbb{E}(A_{ij}, P(w), \Omega)$ (left), vs. $\lambda = -0.94$ under $\mathbb{E}(A_{ij}, \Omega)$ (right). (c)-(d) Ecological networks ECO1 and ECO2, analyzed via $\mathbb{E}(A_{ij}, P(w), \Omega)$ (left) vs. $\mathbb{E}(A_{ij}, \Omega)$ (right), taking Ω from our Ecological dynamics. Once again we find that while the random J is unstable ($\lambda = 186$ and 227) once the dynamics is properly treated through Ω the system is found to be stable ($\lambda = -16.0$ and -289). (e)-(f) The biological networks PPI1 and PPI2 are matched with three potential J matrices: random ($\mathbb{E}(A_{ij}, P(w), C)$, left), Biochemical ($\mathbb{E}(A_{ij}, \Omega_1)$, center) and Regulatory ($\mathbb{E}(A_{ij}, \Omega_2)$, right). This exemplifies the fact that under the dynamics ensemble $\mathbb{E}(A_{ij}, \Omega)$ the same network can lead to different dynamics behaviors, *i.e.* distinct J , owing to the nonlinear interaction mechanisms (Biochemical vs. Regulatory). Also here we find that while the random J is unstable ($\lambda = 6.23, 10.3 > 0$), our dynamic J matrices all have $\lambda < 0$, excluded from the diversity-stability paradox. In all panels when displaying J each entry (pixel) represents an average over a 50×50 block of the complete Jacobian matrix. Details on all 6 empirical networks are provided in Supplementary Section 4.

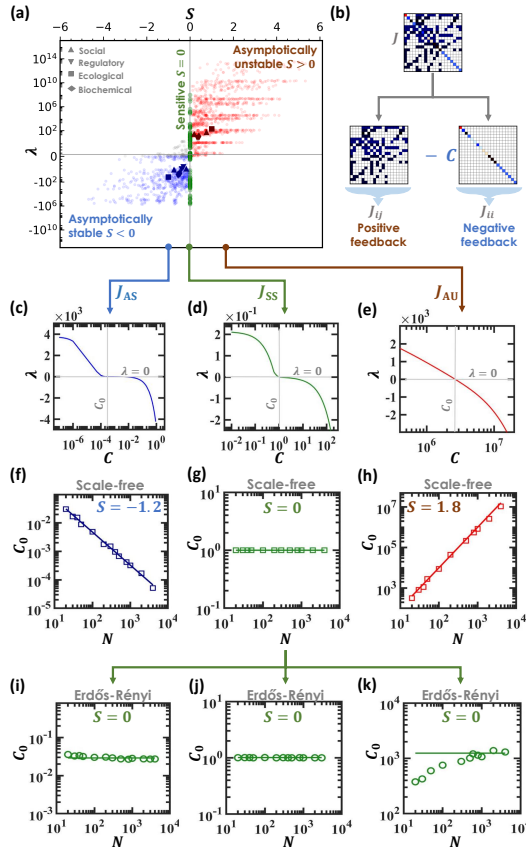


Figure 4: **Three classes of dynamic stability in real and model networks.** We extracted 2,077 Jacobian matrices from the $\mathbb{E}(A_{ij}, \Omega)$ ensemble, using combinations of model/real networks with different dynamic exponents Ω . For each J we calculated the principal eigenvalue λ and the stability classifier S in (3.31). (a) λ vs. S for all 2,077 J -matrices. We observe the three predicted classes: Asymptotically unstable (red) in which $S > 0$ and hence also $\lambda > 0$; Sensitively stable (green), where $S = 0$ and λ can be both positive or negative; Asymptotically stable (blue), where $S < 0$ and therefore $\lambda < 0$. Our classification was inaccurate in $\sim 4\%$ of the cases (grey). Empirical networks (solid symbols): Under the random ensemble $\mathbb{E}(A_{ij}, P(w), C)$ all our empirical networks are classified as unstable (red symbols). However, the same networks under $\mathbb{E}(A_{ij}, \Omega)$, each with its relevant Ω , become dynamically stable (blue symbols). Hence, networks rendered unstable via the existing paradigm, are, in fact, stable, when accounting for the nonlinearity through Ω . (b) The value of λ emerges from the competition between J 's off-diagonal terms, representing positive feedback, and the strength of the diagonal terms J_{ii} (negative feedback). Therefore one can force a system towards stability ($\lambda < 0$) by increasing C in (7). (c) - (e) Taking three specific J matrices from each class, we plot λ vs. C , seeking the critical C_0 , in which λ becomes negative (grey lines). (f) For the stable J_{AS} ($S = -1.2$) we find that C_0 decreases with N (squares), capturing the asymptotic stability, in which for large systems ($N \rightarrow \infty$) stability is sustained even under arbitrarily small C . The theoretical scaling predicted in Eq. (11) is also shown (solid line, slope -1.2). (g) For J_{SS} we have $S = 0$, the critical C_0 is independent of N , hence the system's stability can be affected by finite changes to its dynamic parameters, *e.g.*, environmental perturbations. (h) The asymptotically unstable J_{AU} ($S = 1.8$) has $C_0 \rightarrow \infty$ in the limit of large N , in perfect agreement with Eq. (11) (solid line). (i) - (k) For a bounded $P(k)$, *e.g.*, Erdős-Rényi, β vanishes and hence $S = 0$ in (3.31). Under these conditions, regardless of Ω , the system is always sensitively stable and therefore C_0 does not scale with N . This demonstrates the role of degree-heterogeneity in ensuring stability, in the face of changing environmental conditions.

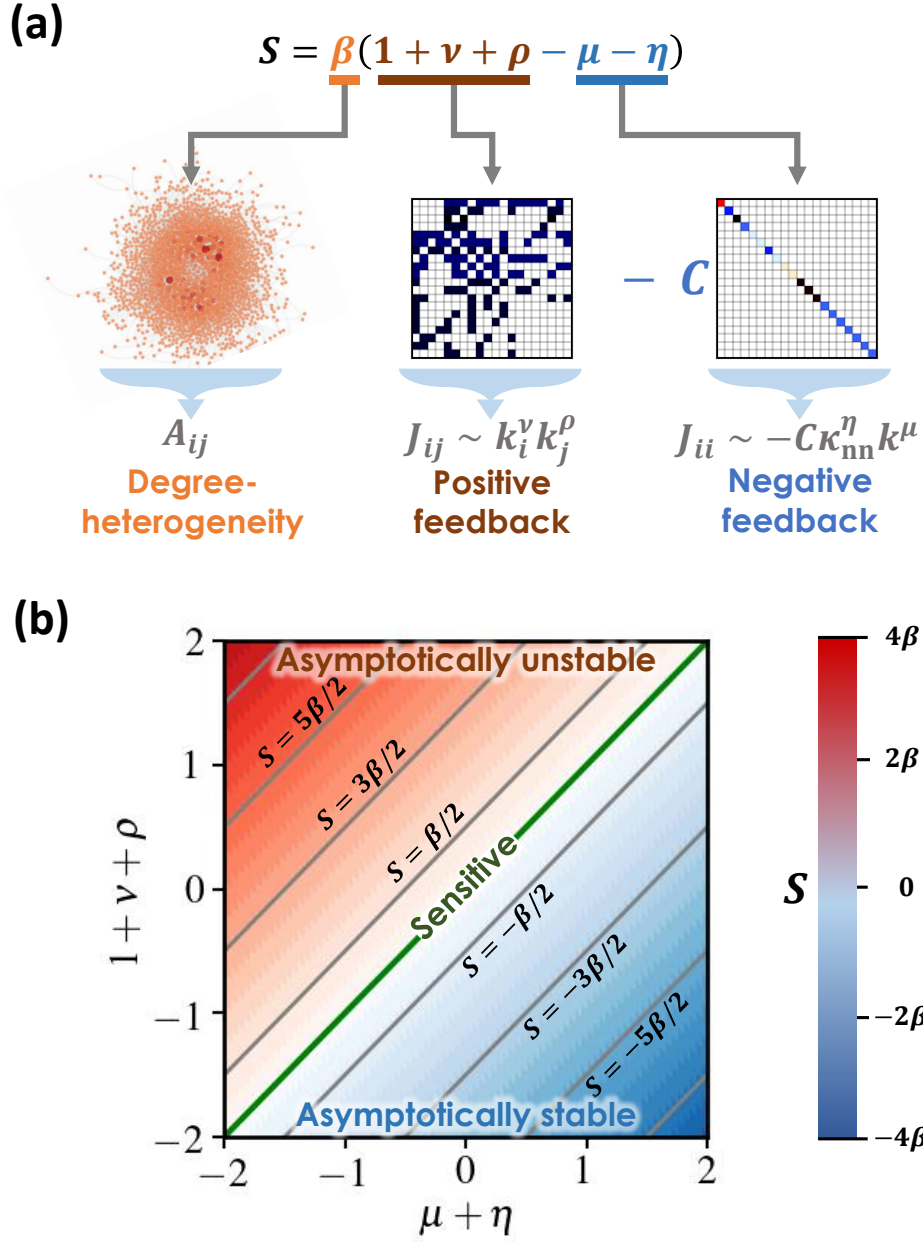


Figure 5: **The ingredients of dynamic stability.** (a) The stability classifier S (3.31) comprises five exponents: β characterizes the network topology and its degree heterogeneity via (3.2); ν, ρ determine the magnitude of J 's off-diagonal terms; μ, η characterize the self-dynamic diagonal terms. This portrays stability as a balance between the positive feedback mediated by the system's interactions, strengthened with increasing ν, ρ , vs. the stabilizing effect of the diagonal terms, that are reinforced by η, μ . (b) S vs. the exponents $\Omega = (\eta, \mu, \nu, \rho)$. Increasing ν, ρ drives the system towards the unstable class ($S > 0$), while increasing μ, η enhances the system's stability. In addition to the discrete classification of stable dynamics (blue, $S < 0$), unstable dynamics (red, $S > 0$) and sensitive dynamics (green, $S = 0$), S also helps quantify the continuum *level* of stability, where the more negative/positive is S , the more stable/unstable is the system. Grey lines represent equi-stable systems.

References

- [1] S.V. Buldyrev, R. Parshani, G. Paul, H.E. Stanley and S. Havlin. Catastrophic cascade of failures in interdependent networks. *Nature*, 464:1025–1028, 2010.
- [2] I. Dobson, B.A. Carreras, V.E. Lynch and D.E. Newman. Complex systems analysis of series of blackouts: Cascading failure, critical points, and self-organization. *Chaos*, 17:026103, 2007.
- [3] D. Duan, C. Lv, S. Si, Z. Wang, D. Li, J. Gao, S. Havlin, H.E. Stanley and S. Boccaletti. Universal behavior of cascading failures in interdependent networks. *Proc. Natl. Acad. Sci. USA*, 116:22452–57, 2019.
- [4] A.E. Motter and Y.-C. Lai. Cascade-based attacks on complex networks. *Physical Review E*, 66:065102, 2002.
- [5] P. Crucitti, V. Latora and M. Marchiori. Model for cascading failures in complex networks. *Phys. Rev. E*, 69:045104–7, 2004.
- [6] D. Achlioptas, R.M. D’Souza and J. Spencer. Explosive percolation in random networks. *Science*, 323:1453–1455, 2009.
- [7] J. Gao, B. Barzel and A.-L. Barabási. Universal resilience patterns in complex networks. *Nature*, 530:307–312, 2016.
- [8] S. Boccaletti, J.A. Almendral, S. Guana, I. Leyvad, Z. Liua, I.S. Nadal, Z. Wang and Y. Zou. Explosive transitions in complex networks structure and dynamics: Percolation and synchronization. *Physics Reports*, 660:1–94, 2016.
- [9] S. Boccaletti, V. Latora, Y. Moreno, M. Chavez and D.-U. Hwang. Complex networks: Structure and dynamics. *Physics Reports*, 424:175–308, 2006.
- [10] Michael M Danziger, Ivan Bonamassa, Stefano Boccaletti, and Shlomo Havlin. Dynamic interdependence and competition in multilayer networks. *Nature Physics*, 15(2):178–185, 2019.
- [11] K.Z. Coyote¹, J. Schluter¹ and K.R. Foster¹. The ecology of the microbiome: Networks, competition, and stability. *Science*, 350:663–666, 2015.
- [12] D. Tilman, P.B. Reich and J.M.H. Knops. Biodiversity and ecosystem stability in a decade-long grassland experiment. *Nature*, 441:629632, 2006.
- [13] R.V. Solé and J.M. Montoya. Complexity and fragility in ecological networks. *Proc. R. Soc. London Ser. B*, 268:2039–2045, 2001.
- [14] H.I. Schreier, Y. Soen and N. Brenner. Exploratory adaptation in large random networks. *Nature Communications*, 8:14826, 2017.
- [15] L.M. Pecora and T.L. Carroll. Master stability functions for synchronized coupled systems. *Phys. Rev. Lett.*, 80:2109, 1998.
- [16] R.M. May. Will a large complex system be stable? *Nature*, 238:413 – 414, 1972.
- [17] G. Caldarelli. *Scale-free networks: complex webs in nature and technology*. Oxford University Press, New York, 2007.
- [18] A.-L. Barabási, H. Jeong, E. Ravasz, Z. Nédá, A. Schubert and T. Vicsek. *Physica A*, 311:590, 2002.
- [19] D.J. Watts and S.H. Strogatz. Collective dynamics of ‘small-world’ networks. *Nature*, 393:440–442, 1998.
- [20] B. Barzel and O. Biham. Quantifying the connectivity of a network: The network correlation function method. *Phys. Rev. E*, 80:046104–15, 2009.
- [21] A.-L. Barabási and R. Albert. Emergence of scaling in random networks. *Science*, 286:509–512, 1999.
- [22] M.E.J. Newman. *Networks - an introduction*. Oxford University Press, New York, 2010.
- [23] S. Allesina and S. Tang. Stability criteria for complex ecosystems. *Nature*, 483:205208, 2012.
- [24] W. Tarnowski, I. Neri and P. Vivo. Universal transient behavior in large dynamical systems on networks. *Phys. Rev. Research*, 2:023333, 2020.
- [25] S. Suweis, F. Simini, J.R. Banavar and A. Maritan. Emergence of structural and dynamical properties of ecological mutualistic networks. *Nature*, 500(7463):449–452, 2013.
- [26] W. Feng and K. Takemoto. Heterogeneity in ecological mutualistic networks dominantly determines community stability. *Scientific reports*, 4:5912, 2014.

- [27] A. Mougi and M. Kondoh. Diversity of interaction types and ecological community stability. *Science*, 337(6092):349–351, 2012.
- [28] T. Okuyama and J.N. Holland. Network structural properties mediate the stability of mutualistic communities. *Ecology Letters*, 11(3):208–216, 2008.
- [29] E. Thébault and C. Fontaine. Stability of ecological communities and the architecture of mutualistic and trophic networks. *Science*, 329(5993):853–856, 2010.
- [30] D. Gravel, F. Massol and M.A. Leibold. Stability and complexity in model meta-ecosystems. *Nature Communications*, 7(12457):1–8, 2016.
- [31] Sitabhra Sinha and Sudeshna Sinha. Evidence of universality for the may-wigner stability theorem for random networks with local dynamics. *Physical Review E*, 71(2):020902, 2005.
- [32] G. Yan, N.D. Martinez and Y.-Y. Liu. Degree heterogeneity and stability of ecological networks. *Journal of The Royal Society Interface*, 14:131, 2017.
- [33] C. Jacquet, C. Moritz, L. Morissette, P. Legagneux, F. Massol, P. Archambault and D. Gravel. No complexity-stability relationship in empirical ecosystems. *Nature Communications*, 7:12573, 2016.
- [34] K.S. McCann. The diversity–stability debate. *Nature*, 405(6783):228–233, 2000.
- [35] B. Barzel and A.-L. Barabási. Universality in network dynamics. *Nature Physics*, 9:673 – 681, 2013.
- [36] U. Harush and B. Barzel. Dynamic patterns of information flow in complex networks. *Nature Communications*, 8:2181, 2017.
- [37] C. Hens, U. Harush, R. Cohen, S. Haber and B. Barzel . Spatiotemporal propagation of signals in complex networks. *Nature Physics*, 15:403, 2019.
- [38] R. Pastor-Satorras, C. Castellano, P. Van Mieghem and A. Vespignani. Epidemic processes in complex networks. *Rev. Mod. Phys.*, 87:925–958, 2015.
- [39] P.S. Dodds, R. Muhamad and D.J. Watts. An experimental study of search in global social networks. *Science*, 301:827–829, 2003.
- [40] D. Brockmann, V. David and A.M. Gallardo. Human mobility and spatial disease dynamics. *Reviews of Nonlinear Dynamics and Complexity*, 2:1, 2009.
- [41] G. Karlebach and R. Shamir. Modelling and analysis of gene regulatory networks. *Nature Reviews*, 9:770–780, 2008.
- [42] J.D. Murray. *Mathematical Biology*. Springer, Berlin, 1989.
- [43] B. Barzel and O. Biham. Binomial moment equations for stochastic reaction systems. *Phys. Rev. Lett.*, 106:150602–5, 2011.
- [44] B. Barzel and O. Biham. Stochastic analysis of complex reaction networks using binomial moment equations. *Phys. Rev. E*, 86:031126, 2012.
- [45] C.S. Holling. Some characteristics of simple types of predation and parasitism. *The Canadian Entomologist*, 91:385–398, 1959.
- [46] J.N. Holland, D.L. DeAngelis and J.L. Bronstein. Population dynamics and mutualism: functional responses of benefits and costs. *American Naturalist*, 159:231–244, 2002.
- [47] E.L. Berlow, J.A. Dunne, N.D. Martinez, P.B. Stark, R.J. Williams and U. Brose. Simple prediction of interaction strengths in complex food webs. *Proceedings of the National Academy of Sciences*, 106:187–191, 2009.
- [48] J.F. Hayes and T.V.J. Ganesh Babu. *Modeling and Analysis of Telecommunications Networks*. John Wiley & Sons, Inc., Hoboken, NJ, USA, 2004.
- [49] A.-L. Barabási and Z.N. Oltvai. Network biology: understanding the cell’s functional organization. *Nat. Rev. Gen.*, 5:101, 2004.
- [50] T. Opsahl and P. Panzarasa. Clustering in weighted networks. *Social Networks*, 31:155–163, 2009.
- [51] J.-P. Eckmann, E. Moses and D. Sergi. Entropy of dialogues creates coherent structures in e-mail traffic. *Proc. Natl. Acad. Sci. USA*, 101:14333–7, 2004.
- [52] M. Faloutsos, P. Faloutsos and C. Faloutsos. On power-law relationships of the Internet topology. *Comput. Commun. Rev.*, 29:251–262, 1999.

- [53] G. Caldarelli and M. Catanzaro. *Networks: A very short introduction*. Oxford University Press, New York, 2012.
- [54] M. Boguñá, R. Pastor-Satorras and A. Vespignani. Absence of epidemic threshold in scale-free networks with degree correlations. *Phys. Rev. Lett.*, 90:028701–4, 2003.
- [55] R.M. May. *Theoretical Ecology: Principles and Application*, 1:78–104, 1976.
- [56] J.A. Almendral and A. Díaz-Guilera. Dynamical and spectral properties of complex networks. *New Journal of Physics*, 9:187–187, 2007.
- [57] P. Van Mieghem. Epidemic phase transition of the SIS type in network. *Europhysics Letters*, 97(4):48004, 2012.
- [58] P. Van Mieghem. *Graph Spectra for Complex Networks*. Cambridge University Press, Cambridge, UK, 2010.
- [59] V.S. Afraimovich and L.A. Bunimovich. Dynamical networks: interplay of topology, interactions and local dynamics. *Nonlinearity*, 20:1761–1771, 2007.
- [60] C. Kirst, M. Timme and D. Battaglia. Dynamic information routing in complex networks. *Nature Communications*, 7:11061, 2016.
- [61] A. Barrat, M. Barthélemy and A. Vespignani. *Dynamical Processes on Complex Networks*. Cambridge University Press, Cambridge, 2008.
- [62] G. Yan, G. Tsekenis, B. Barzel, J.-J. Slotine, Y.-Y. Liu and A.-L. Barabási. Spectrum of controlling and observing complex networks. *Nature Physics*, 11:779786, 2015.
- [63] L. Schmetterer and K. Sigmund (Eds.). *Hans Hahn Gesammelte Abhandlungen Band 1/Hans Hahn Collected Works Volume 1*. Springer, Vienna, Austria, 1995.
- [64] H. Yu *et al.* High-quality binary protein interaction map of the yeast interactome network. *Science*, 322:104–110, 2008.
- [65] J.F. Rual *et al.* Towards a proteome-scale map of the human protein-protein interaction network. *Nature*, 437:1173–1178, 2005.
- [66] Interaction web database. <http://www.nceas.ucsb.edu/interactionweb/resources>.
- [67] S. Milojević. Power-law distributions in information science: making the case for logarithmic binning. *Journal of the American Society for Information Science and Technology*, 61:2417–2425, 2010.

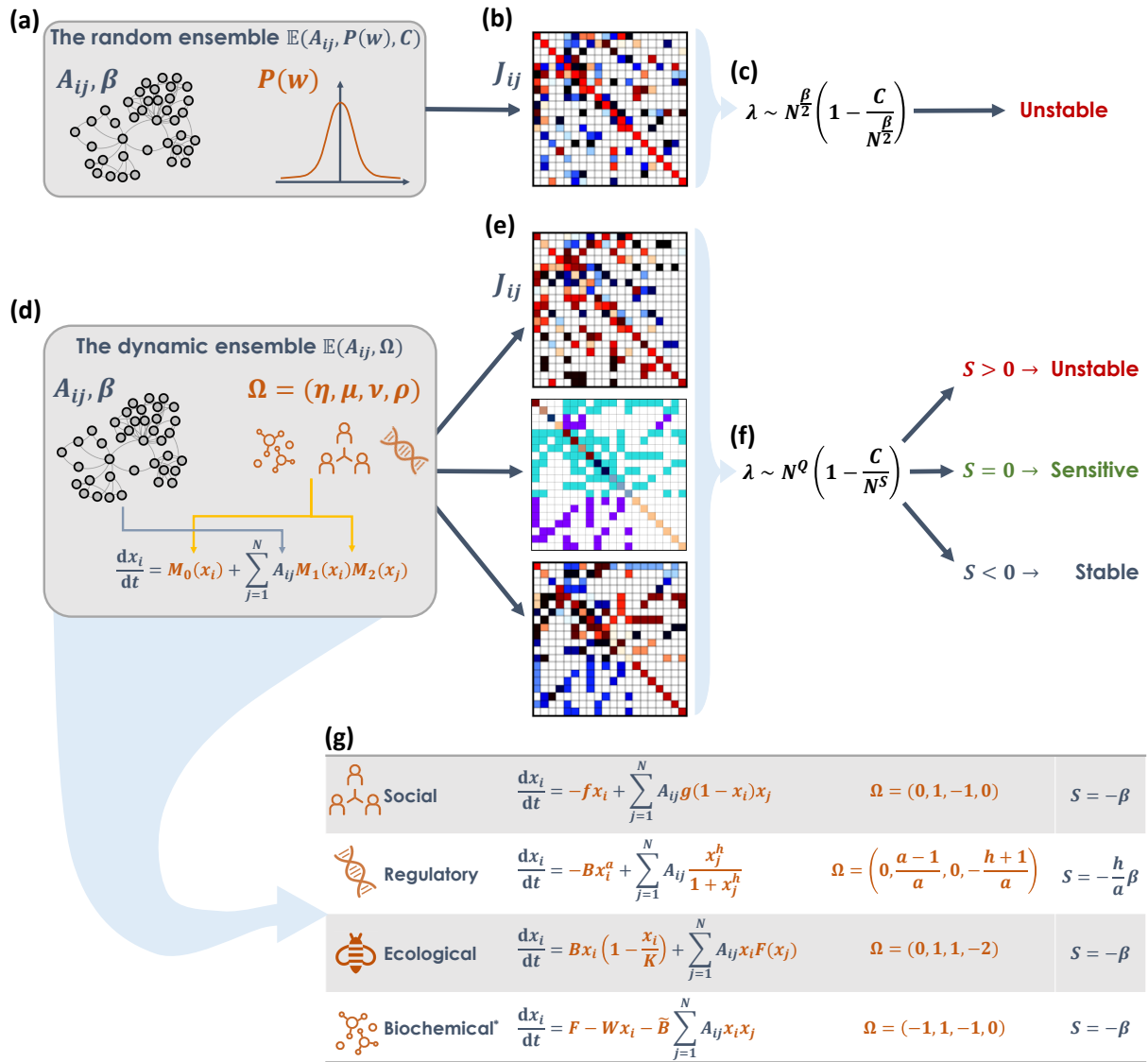


Figure 1 - full size.

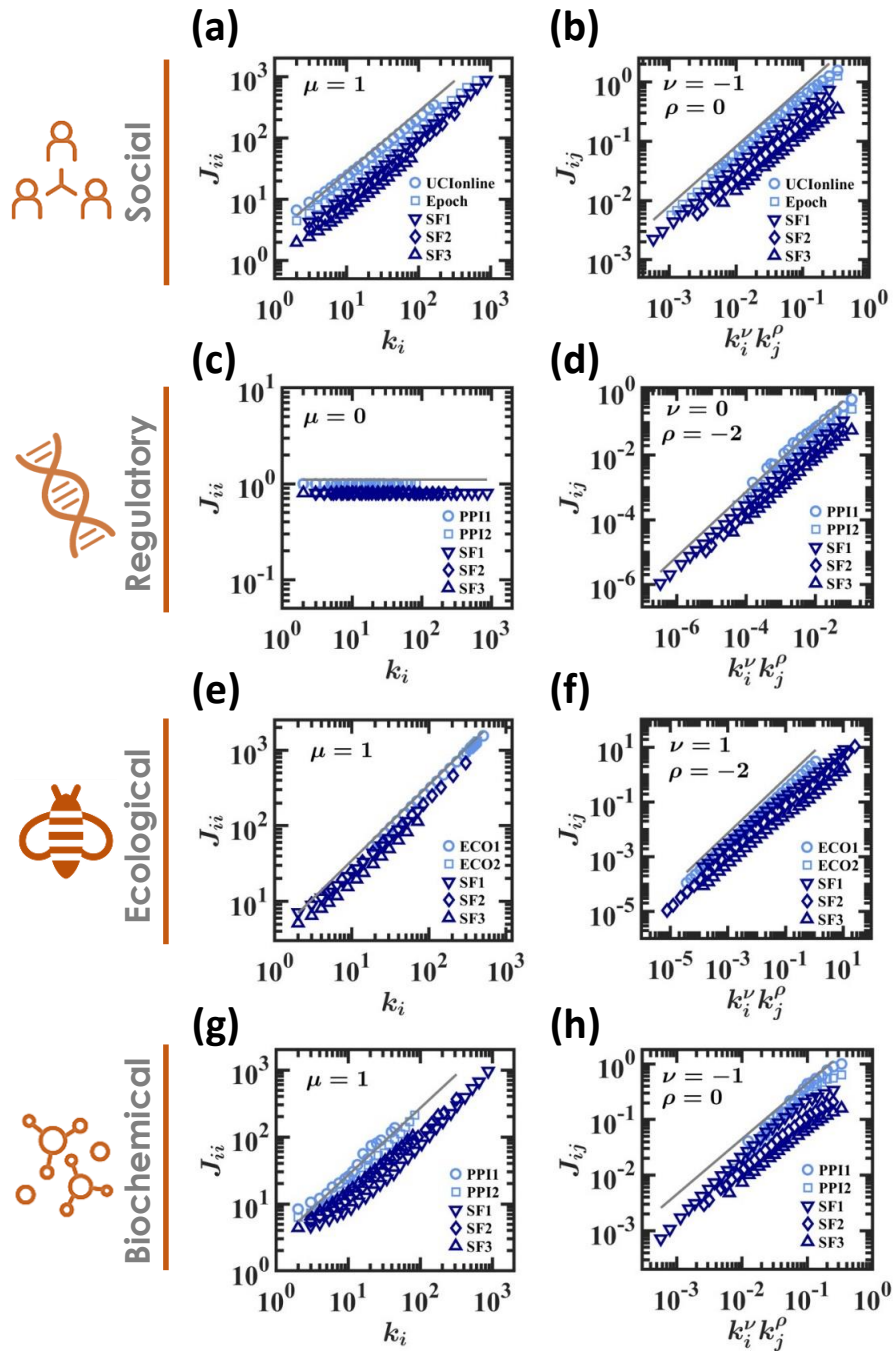


Figure 2 - full size.

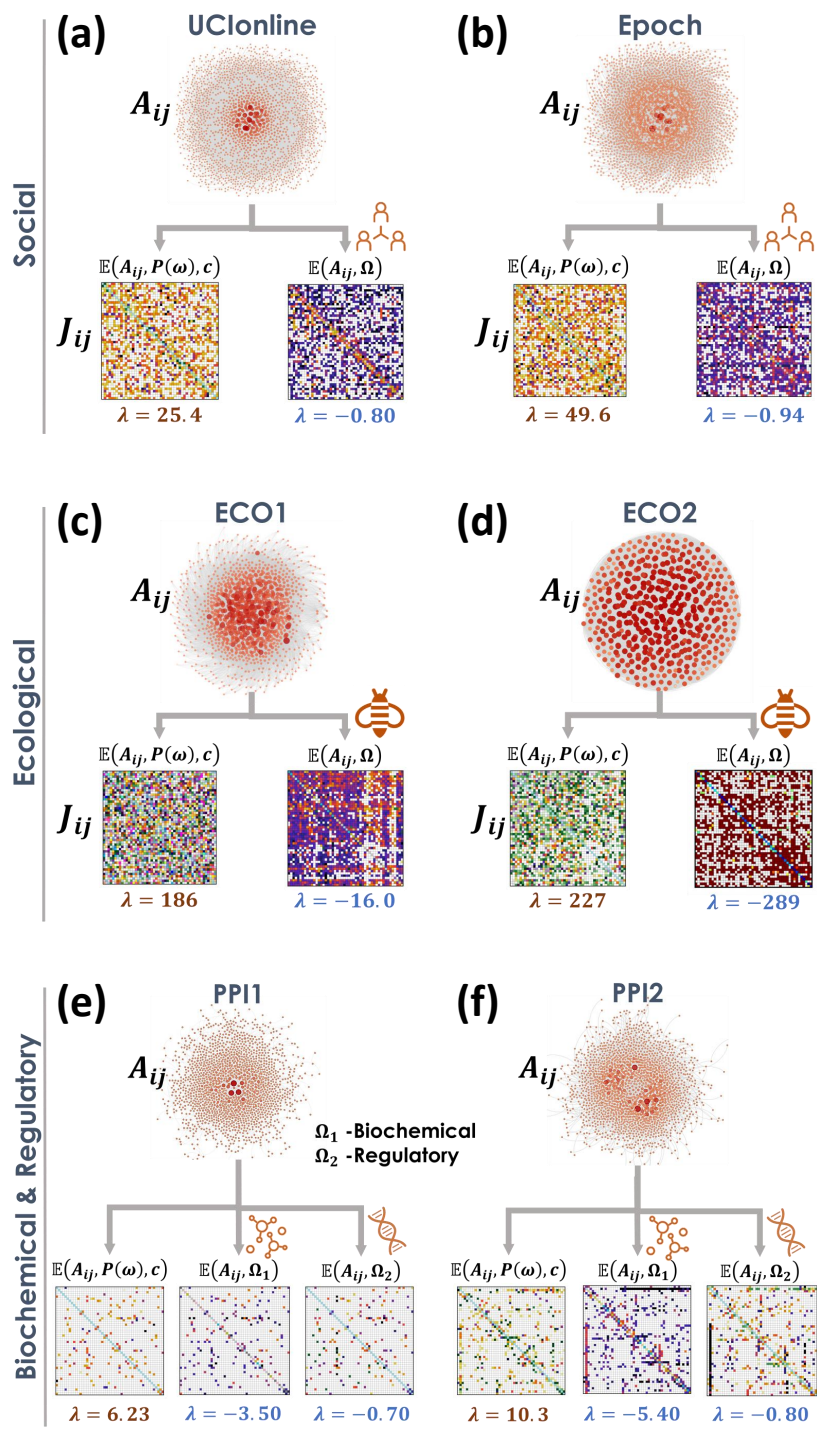


Figure 3 - full size.

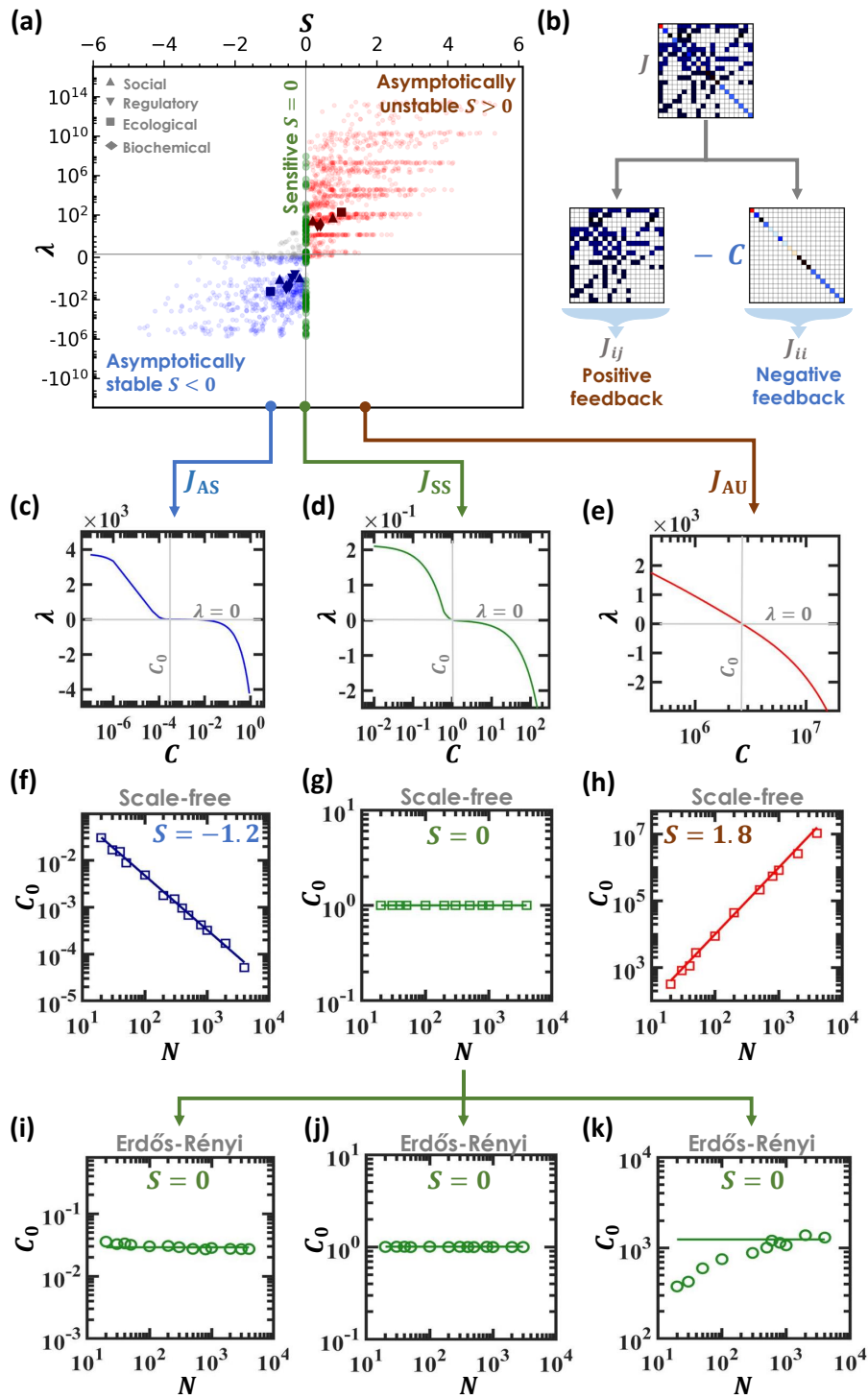


Figure 4 - full size.

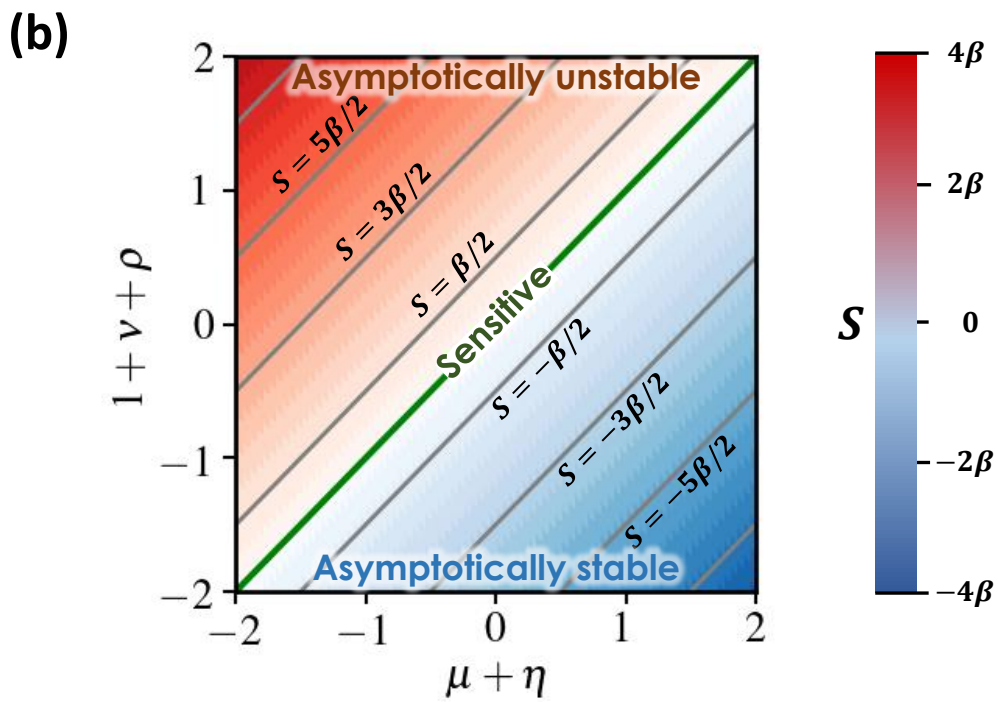
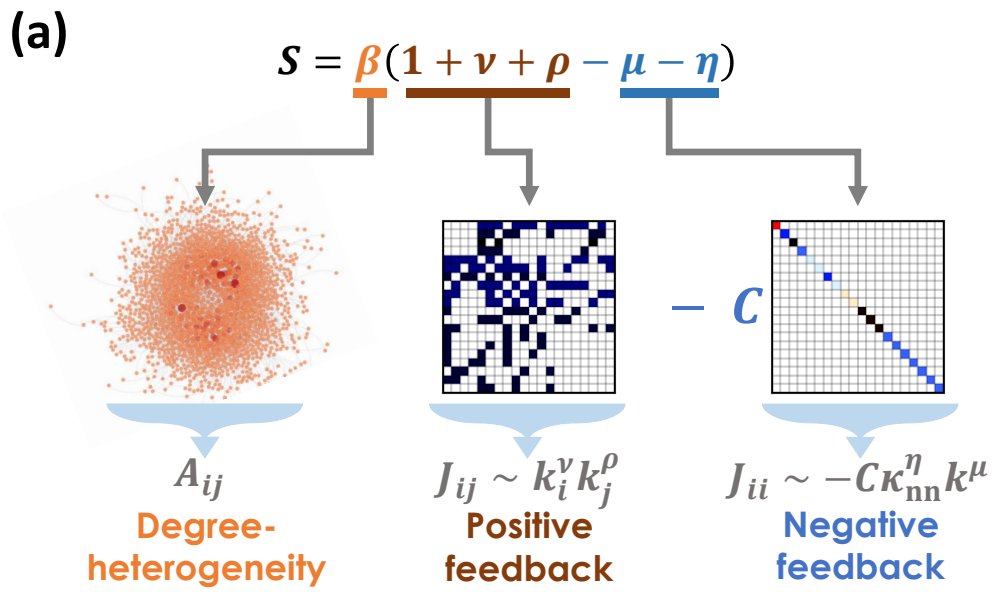


Figure 5 - full size.

Dynamic stability of complex networks

Supplementary information

November 9, 2021

Contents

1	The Jacobian ensemble $\mathbb{E}(A_{ij}, \Omega)$	1
1.1	The fixed-points \mathbf{x}^*	1
1.1.1	Evaluating $\langle M_2(x) \rangle_{\odot}$	3
1.2	Diagonal terms D_{ii}	5
1.3	The off-diagonal terms W_{ij}	7
1.4	Piecing together the J_{ij} puzzle	8
1.4.1	Impact of $P(k)$ and κ_{nn}	9
2	Analyzing the dynamic models	12
2.1	Social dynamics	12
2.2	Regulatory dynamics	13
2.3	Ecological dynamics	15
2.4	Biochemical dynamics	17
3	Principle eigenvalue of $J_{ij} \in \mathbb{E}(A_{ij}, \Omega)$	18
3.1	The role of topology vs. dynamics	22
3.2	Stability classifier S under negative interactions	24
4	Methods and data analysis	25
4.1	Numerical integration	25
4.2	Numerically estimating J_{ij}	26
4.3	Logarithmic binning	26
4.4	Model and empirical networks	27
5	Mixed dynamics	28

1 The Jacobian ensemble $\mathbb{E}(A_{ij}, \Omega)$

To analyze complex system stability we seek the *real* Jacobian matrix J_{ij} , as extracted from the system's specific nonlinear interaction mechanisms. We first rewrite Eq. (6) of the main text as

$$\frac{dx_i}{dt} = F_i(\mathbf{x}(t)), \quad (1.1)$$

where

$$F_i(\mathbf{x}(t)) = M_0(x_i(t)) + \sum_{j=1}^N A_{ij} M_1(x_i(t)) M_2(x_j(t)). \quad (1.2)$$

We denote (1.1)'s fixed-point(s) by $\mathbf{x}^* = (x_1, \dots, x_N)^\top$, where we omit the term t to capture their independence on time. These fixed-points are obtained by solving the equilibrium equation

$$F_i(\mathbf{x}^*) = 0. \quad (1.3)$$

To assess the dynamic stability of each of (1.3)'s solutions we track their response to small perturbations, via the Jacobian

$$J_{ij} = \left. \frac{\partial F_i(\mathbf{x})}{\partial x_j} \right|_{\mathbf{x}=\mathbf{x}^*}, \quad (1.4)$$

whose structure we obtain below. Writing

$$J = A \otimes W - I \otimes D \quad (1.5)$$

we treat separately the diagonal terms $J_{ii} = D_{ii}$ and the off-diagonal terms $J_{ij} = A_{ij} W_{ij}$ (I is the identity matrix and \otimes is the Hadamard product).

1.1 The fixed-points \mathbf{x}^*

We consider systems of the form (1.1) that exhibit at least one fully positive fixed-point \mathbf{x}^* . Using Eq. (1.3) we write

$$M_0(x_i) + \sum_{j=1}^N A_{ij} M_1(x_i) M_2(x_j) = 0, \quad (1.6)$$

which can be expressed as

$$R(x_i) \sum_{j=1}^N A_{ij} M_2(x_j) = 1, \quad (1.7)$$

where

$$R(x_i) = -\frac{M_1(x_i)}{M_0(x_i)}. \quad (1.8)$$

Denoting i 's degree by $k_i = \sum_{j=1}^N A_{ij}$ we write (1.7) as

$$R(x_i) = \frac{1}{k_i \langle M_2(x) \rangle_{i, \odot}}, \quad (1.9)$$

in which

$$\langle M_2(x) \rangle_{i, \odot} = \frac{1}{k_i} \sum_{j=1}^N A_{ij} M_2(x_j) \quad (1.10)$$

represents an average of the function $M_2(x_j)$ over all of node i 's direct network *neighborhood*, which we captured by the \odot symbol. Assuming the function $R(x)$ is invertible around x_i we obtain i 's fixed-point activity as

$$x_i = R^{-1}(q_i), \quad (1.11)$$

where $R^{-1}(x)$ is the inverse function of $R(x)$ and

$$q_i = \frac{1}{k_i \langle M_2(x) \rangle_{i, \odot}} \quad (1.12)$$

is i 's inverse degree, which approaches zero in the limit of large k_i .

To understand the dependence of activity on degree, we seek the average steady-state activity over all nodes with degree k as

$$x(k) = \frac{1}{|\mathbf{G}(k)|} \sum_{i \in \mathbf{G}(k)} x_i, \quad (1.13)$$

where $\mathbf{G}(k) = \{i \in [1, N] | k_i = k\}$ is the group of all nodes with degree k , and $|\mathbf{G}(k)|$ is the number of nodes in that group. To approximate $x(k)$ we first evaluate the average neighborhood activity of all nodes in $\mathbf{G}(k)$ via

$$\langle M_2(x) \rangle_{k, \odot} = \frac{1}{|\mathbf{G}(k)|} \sum_{i \in \mathbf{G}(k)} \langle M_2(x) \rangle_{i, \odot}, \quad (1.14)$$

capturing the average value of $M_2(x)$ surrounding nodes with degree k . Most generally, the activities x_j may depend, to some extent, on the degree k_i of their neighbor i , however this dependence is often unknown, and, most importantly, relatively weak¹. Indeed, i is but one of j 's k_j neighbors, who are typically a random selection, representative of the network's degree distribution². Therefore, i 's degree k_i is only weakly correlated with j 's activity x_j . To capture this dependence we approximate (1.14) as

$$\langle M_2(x) \rangle_{k, \odot} \approx f(k) \langle M_2(x) \rangle_{\odot}, \quad (1.15)$$

where

$$\langle M_2(x) \rangle_{\odot} = \frac{1}{N} \sum_{i=1}^N \frac{1}{k_i} \sum_{j=1}^N A_{ij} M_2(x_j) \quad (1.16)$$

represents the average of the function $M_2(x_j)$ over *all* network neighborhoods, independent of i or k . In (1.15) the term $\langle M_2(x) \rangle_{\odot}$ captures a characteristic aggregated function of the system's fixed-point, capturing the value of $M_2(x_j)$ averaged over all nearest neighbor nodes, but not specifically over i 's neighbors - hence the approximation sign \approx , rather than $=$. The function $f(k)$ corrects this average to account for the fact that in the l.h.s. of (1.15) the average is carried out selectively over nodes whose neighbor has degree k . For example, $f(k) = 1$ represents the *perfect* case of no degree-correlations, under which x_j is fully independent of its neighbor's degree k . More generally, we assume $f(k)$ to be a *weak* function, *i.e.* sub-polynomial in k , for example

$$f(k) \sim \log^n(k). \quad (1.17)$$

We can now approximate $x(k)$ in (1.13), taking x_i from (1.11), and $\langle M_2(x) \rangle_{i,\odot}$ from (1.15) to obtain

$$x(k) = R^{-1}(q), \quad (1.18)$$

where

$$q = \frac{1}{f(k) \langle M_2(x) \rangle_{\odot} k}. \quad (1.19)$$

In the asymptotic limit of large k , the sub-polynomial contribution of $f(k)$ becomes negligible, and hence we have

$$q \sim \langle M_2(x) \rangle_{\odot}^{-1} k^{-1}. \quad (1.20)$$

1.1.1 Evaluating $\langle M_2(x) \rangle_{\odot}$

To link $\langle M_2(x) \rangle_{\odot}$ to the network A_{ij} we use a mean-field approximation. We first define the nearest neighbor activity as

$$x_{\text{nn}} = \langle x \rangle_{\odot} = \frac{1}{N} \sum_{i=1}^N \frac{1}{k_i} \sum_{j=1}^N A_{ij} x_j, \quad (1.21)$$

and its corresponding nearest neighbor degree as

$$\kappa_{\text{nn}} = \langle k \rangle_{\odot} = \frac{1}{N} \sum_{i=1}^N \frac{1}{k_i} \sum_{j=1}^N A_{ij} k_j. \quad (1.22)$$

Hence, the average nearest neighbor node is characterized by activity x_{nn} and degree κ_{nn} . While x_{nn} depends on the system's dynamics (1.1), κ_{nn} is fully determined by the topology A_{ij} , linked to the network's degree distribution $P(k)$. In the absence of degree correlations we have³

$$\kappa_{\text{nn}} = \frac{\langle k^2 \rangle}{\langle k \rangle}, \quad (1.23)$$

with $\langle k^n \rangle$ capturing the n th moment of $P(k)$. For a homogeneous network in which $P(k)$ is bounded we have $\kappa_{\text{nn}} \approx \langle k \rangle$, however, if the network is highly heterogeneous, *i.e.* $P(k)$ is fat-tailed - as indeed, many real networks are⁴ - we find that $\kappa_{\text{nn}} \gg \langle k \rangle$. More generally, in case the network has degree correlations we write⁵

$$\kappa_{\text{nn}} = \sum_{k'=1}^{\infty} \sum_{k=1}^{\infty} k P(k|k') P(k') \quad (1.24)$$

in which the conditional probability $P(k|k')$ captures the dependence between neighboring nodes. In both cases, (1.23) and the more general (1.24), under extreme degree-heterogeneity, κ may diverge with system size as²

$$\kappa_{\text{nn}} \sim N^\beta. \quad (1.25)$$

We can now link $\langle M_2(x) \rangle_{\odot}$ in (1.16) to κ_{nn} and x_{nn} , as, indeed, $\langle M_2(x) \rangle_{\odot}$ is designed to capture the mean value of $M_2(x)$ over all nearest neighbor nodes, namely nodes with typical degree κ_{nn} and activity x_{nn} . We, therefore, approximate (1.16) as

$$\langle M_2(x) \rangle_{\odot} \approx M_2(x_{\text{nn}}), \quad (1.26)$$

in which we swap the order of operations from $\langle M_2(x) \rangle$ to $M_2(\langle x \rangle)$. Such approximation becomes exact in the limit where $M_2(x)$ is linear or when x_j are narrowly distributed. For example, in our Biochemical model we have $M_2(x_j) = x_j$, a linear function, and in our Social model the activities x_j are bounded, hence narrowly distributed between zero and unity. Approximation (1.26) is also justified when $M_2(x)$ is sub-linear, *e.g.*, a saturating function $M_2(x \rightarrow \infty) \rightarrow 1$. Such saturation is present, for instance, in our Regulatory and Ecological dynamics. Under these conditions, even if x_j are broadly distributed, $M_2(x_j)$ are uniform, and hence their average is (roughly) concentrated around $M_2(\langle x \rangle)$. For a super-linear $M_2(x)$, combined with broadly distributed x_j , approximation (1.26) becomes inaccurate.

To evaluate $M_2(x_{\text{nn}})$'s dependence on κ_{nn} we use (1.9) to write

$$R(x_{\text{nn}}) = \frac{1}{\kappa_{\text{nn}} f(\kappa_{\text{nn}}) M_2(x_{\text{nn}})}, \quad (1.27)$$

where we substitute $\langle M_2(x) \rangle_{i,\odot}$ by $f(\kappa_{\text{nn}}) M_2(x_{\text{nn}})$ following approximations (1.15) and (1.26), and use the nearest neighbor degree κ_{nn} in place of k . We therefore arrive at

$$Z(x_{\text{nn}}) = \frac{1}{f(\kappa_{\text{nn}}) \kappa_{\text{nn}}} \equiv q_{\odot}, \quad (1.28)$$

where $Z(x) = R(x) M_2(x)$ is a dynamic function, fully determined by $M_0(x)$, $M_1(x)$ and $M_2(x)$ in (1.1). In (1.29) we use the notation q_{\odot} to signify the inverse degree (q) associated with the typical *neighborhood* (\odot). By inversion we obtain

$$x_{\text{nn}} = Z^{-1}(q_{\odot}), \quad (1.29)$$

and hence

$$M_2(x_{\text{nn}}) = M_2(Z^{-1}(q_{\odot})). \quad (1.30)$$

To obtain the asymptotic scaling of $M_2(x_{\text{nn}})$ on κ_{nn} we use the Hahn expansion⁶ to express $Z(x)$ in the form of a power series around $q_{\odot} \rightarrow 0$, *i.e.* $\kappa_{\text{nn}} \rightarrow \infty$. Hence we write

$$M_2(Z^{-1}(q_{\odot})) = \sum_{n=0}^{\infty} G_n q_{\odot}^{\Psi(n)}, \quad (1.31)$$

where $\Psi(n)$ is a set of real powers in ascending order with n . In the limit of large κ_{nn} (small q_{\odot}) the expansion in (1.31) is dominated by the leading power $\Psi(0)$, predicting that

$$M_2(x_{\text{nn}}) \sim \kappa_{\text{nn}}^{\xi}, \quad (1.32)$$

where

$$\xi = -\Psi(0). \quad (1.33)$$

The exponent ξ is fully determined by the dynamic functions $M_0(x)$, $M_1(x)$ and $M_2(x)$ through the Hahn expansion in (1.31). It is independent of A_{ij} , as well as of other microscopic parameters, such as the specific rate-constants used in (1.1), which are encapsulated within the *coefficients* G_n , but have no impact on the *powers* $\Psi(n)$.

Using approximation (1.26) we substitute $M_2(x_{\text{nn}})$ in (1.32), to replace the $\langle M_2(x) \rangle_{\odot}$ term in the denominator of Eq. (1.19), obtaining

$$q \sim \kappa_{\text{nn}}^{-\xi} k^{-1}. \quad (1.34)$$

Next we use these results, specifically (1.18) and (1.34), to obtain the terms of the Jacobian, J_{ij} and J_{ii} , and their dependence on κ_{nn} and k .

1.2 Diagonal terms D_{ii}

Using (1.2) and (1.4) we write the diagonal Jacobian terms as

$$D_{ii} = \left. \frac{\partial F_i(\mathbf{x})}{\partial x_i} \right|_{\mathbf{x}=\mathbf{x}^*} = \left(M_0'(x_i) + M_1'(x_i) \sum_{j=1}^N A_{ij} M_2(x_j) \right) \Big|_{\mathbf{x}=\mathbf{x}^*}, \quad (1.35)$$

where $M_0'(x) = \partial M_0 / \partial x$ and $M_1'(x) = \partial M_1 / \partial x$. Next we use (1.10) to express the sum on the r.h.s. obtaining

$$D_{ii} = M_0'(x_i) \Big|_{\mathbf{x}=\mathbf{x}^*} + M_1'(x_i) k_i \langle M_2(x) \rangle_{i,\odot} \Big|_{\mathbf{x}=\mathbf{x}^*}, \quad (1.36)$$

in which we substitute the summation by the neighbor average $\langle M_2(x) \rangle_{i,\odot}$. Finally, expressing the fixed-point \mathbf{x}^* via (1.11) and averaging over all nodes with degree k as done in (1.13) - (1.19), we arrive at

$$D(k) = M'_0(R^{-1}(q)) + kM'_1(R^{-1}(q))f(k)\langle M_2(x) \rangle_{\odot}, \quad (1.37)$$

capturing the average diagonal term D_{ii} , associated with a node $i \in \mathbf{G}(k)$.

Next we use (1.8) to write $M_0(x) = -M_1(x)/R(x)$, which provides

$$M'_0(x) = -\frac{M'_1(x)}{R(x)} + \frac{M_1(x)R'(x)}{R^2(x)}. \quad (1.38)$$

Substituting (1.38) and (1.19) into (1.37) we arrive at

$$D(k) = -\frac{M'_1(R^{-1}(q))}{q} + \frac{M_1(R^{-1}(q))R'(R^{-1}(q))}{q^2} + \frac{M'_1(R^{-1}(q))}{q}, \quad (1.39)$$

where we used the fact that $R(R^{-1}(q)) = q$. Collecting all terms we write

$$D(k) = \frac{1}{q^2}Y(R^{-1}(q)), \quad (1.40)$$

where $Y(x) = M_1(x)R'(x)$, similar to $Z(x)$ above, is a dynamic function fully determined by $M_0(x)$ and $M_1(x)$, independent of A_{ij} .

To obtain the asymptotic scaling of $D(k)$ with k we, once again, use the Hahn expansion to express $Y(x)$ in the form of a power series around $q \rightarrow 0$, *i.e.* $k \rightarrow \infty$. Writing

$$Y(R^{-1}(q)) = \sum_{n=0}^{\infty} C_n q^{\Gamma(n)}, \quad (1.41)$$

we obtain the leading power in the expansion of $D(k)$ as $D(k) \sim q^{-2+\Gamma(0)}$, exact up to higher powers in q , which vanish under $q \rightarrow 0$. Using the scaling of Eq. (1.34), this predicts

$$D(k) \sim \kappa_{\text{nn}}^{\xi\mu} k^{\mu}, \quad (1.42)$$

where

$$\mu = 2 - \Gamma(0), \quad (1.43)$$

and ξ is taken from (1.33).

Equation (1.42), valid in the limit of large κ_{nn} and k , captures the typical magnitude of the diagonal terms D_{ii} , and their dependence on each node i 's degree k_i . The scaling exponents μ and ξ are fully determined by $\Gamma(n)$ in (1.41) and $\Psi(n)$ in (1.31), namely they are affected by the *powers* of the dynamic functions $M_0(x)$ and $M_1(x)$. At the same time μ and ξ are independent of the *coefficients* C_n, G_n , hence they are not sensitive to specific parameters, such as rate constants in (1.1). While Eq. (1.42) provides the *scaling* with k , $D(k)$'s specific magnitude may, generally, depend on the coefficients, however for sufficiently large k , such dependencies have little impact

on the spectrum of J_{ij} . Finally, the sign of $D(k)$, positive or negative, is determined by $Y(x)$, which, in turn depends on $M_0(x)$ and $M_1(x)$. Stability can only be ensured in case $D(k) < 0$, *i.e.* negative self-feedback, and hence below we write

$$D(k) \sim -C\kappa_{nn}^{\xi\mu}k^\mu, \quad (1.44)$$

where $C > 0$ (see more detailed discussion in Sec. 1.4).

1.3 The off-diagonal terms W_{ij}

The off-diagonal Jacobian terms are given by

$$W_{ij} = \left. \frac{\partial F_i(\mathbf{x})}{\partial x_j} \right|_{\mathbf{x}=\mathbf{x}^*} = \left. \frac{\partial}{\partial x_j} \left(M_0(x_i) + M_1(x_i) \sum_{j=1}^N A_{ij} M_2(x_j) \right) \right|_{\mathbf{x}=\mathbf{x}^*}. \quad (1.45)$$

Collecting only the terms that explicitly depend on x_j we obtain

$$W_{ij} = M_1(x_i) A_{ij} M_2'(x_j) \Big|_{\mathbf{x}=\mathbf{x}^*}, \quad (1.46)$$

which, taking the fixed-point activities from (1.11) provides

$$W_{ij} = M_1(R^{-1}(q_i)) A_{ij} M_2'(R^{-1}(q_j)). \quad (1.47)$$

We seek the average dependence of W_{ij} on the degrees k_i and k_j , hence we consider the group $\mathbf{G}(k_1, k_2) = \{(i, j) | k_i = k_1; k_j = k_2; A_{ij} = 1\}$, comprising all links ($A_{ij} = 1$) linking nodes with degrees k_1, k_2 . We then average over the relevant Jacobian term as

$$W(k_1, k_2) = \frac{1}{|\mathbf{G}(k_1, k_2)|} \sum_{(i,j) \in \mathbf{G}(k_1, k_2)} W_{ij}, \quad (1.48)$$

allowing us to evaluate the magnitude of an average (non zero) term whose row index is associated with a node of degree k_1 , and whose column index is associated with a node of degree k_2 . Using (1.46) we write

$$W(k_1, k_2) = \frac{1}{|\mathbf{G}(k_1, k_2)|} \sum_{(i,j) \in \mathbf{G}(k_1, k_2)} M_1(x_i) A_{ij} M_2'(x_j) = \langle M_1(x_i) M_2'(x_j) \rangle_{\mathbf{G}(k_1, k_2)}, \quad (1.49)$$

a product average over all node pairs in $\mathbf{G}(k_1, k_2)$. In case the two activities x_i and x_j are uncorrelated, we can approximate the r.h.s. of (1.49) by a product over the single averages, *i.e.* $\langle M_1(x_i) \rangle_{\mathbf{G}(k_1, k_2)} \langle M_2'(x_j) \rangle_{\mathbf{G}(k_1, k_2)}$. Each of these averages can be then evaluated by

$$\langle M_1(x_i) \rangle_{\mathbf{G}(k_1, k_2)} \approx M_1(R^{-1}(q_1)) \quad (1.50)$$

$$\langle M_2'(x_j) \rangle_{\mathbf{G}(k_1, k_2)} \approx M_2'(R^{-1}(q_2)), \quad (1.51)$$

where we use the fact that in $\mathbf{G}(k_1, k_2)$ the activity x_i is on average $R^{-1}(q_1)$, *i.e.* $x(k_1)$ (1.13),

and the activity x_j is $R^{-1}(q_2)$, namely $x(k_2)$. In reality, however, the two activities are, to some extent, correlated by virtue of being nearest neighbors ($A_{ij} = 1$). We therefore follow a similar track as in (1.15) and write (1.49) as

$$W(k_1, k_2) \approx f(k_1, k_2)M_1(R^{-1}(q_1))M_2'(R^{-1}(q_2)), \quad (1.52)$$

capturing the k_1, k_2 correlations via the sub-polynomial function $f(k_1, k_2)$.

We can now obtain the scaling of $W(k_1, k_2)$ by examining the behavior of $M_1(R^{-1}(q_1))$ and $M_2'(R^{-1}(q_2))$ in the limit of large k_1 and k_2 , or subsequently small q_1, q_2 . We, therefore express these functions via the Hahn expansion as

$$M_1(R^{-1}(q)) = \sum_{n=0}^{\infty} K_n q^{\Pi(n)} \quad (1.53)$$

$$M_2'(R^{-1}(q)) = \sum_{n=0}^{\infty} L_n q^{\Theta(n)}, \quad (1.54)$$

and take only the leading term in the limit $q \rightarrow 0$, providing

$$W(k_1, k_2) = f(k_1, k_2)K_0q_1^{\Pi(0)}L_0q_2^{\Theta(0)} + \dots \quad (1.55)$$

As we are only interested in the asymptotic scaling with k_1, k_2 we neglect all terms that do not contribute the scaling, namely $f(k_1, k_2), K_0$ and L_0 . Finally, substituting q with $\kappa_{\text{nn}}^{-\xi}k^{-1}$ as per Eq. (1.34), we obtain

$$W(k_1, k_2) \sim \kappa_{\text{nn}}^{\xi(\nu+\rho)}k_1^{\nu}k_2^{\rho} \quad (1.56)$$

where

$$\nu = -\Pi(0), \quad \rho = -\Theta(0), \quad (1.57)$$

and ξ is taken from (1.33).

1.4 Piecing together the J_{ij} puzzle

We have now obtained the interplay between structure and dynamics, expressed through the magnitude of the diagonal/off-diagonal Jacobian entries, and their dependence on the network's degree distribution via k_i, k_j and κ_{nn} . This dependence is given in terms of asymptotic scaling relationships, as captured by the model dependent exponents μ, ν, ρ, ξ . This leaves a degree of freedom, determined by the specific parameters of each model to add an arbitrary coefficient as a pre-factor to the actual J_{ij} terms. For example, the expression $D(k) \sim -C\kappa_{\text{nn}}^{\xi\mu}k^{\mu}$ in Eq. (1.42) should be taken to mean

$$D(k) = -C(\kappa_{\text{nn}}, k)\kappa_{\text{nn}}^{\xi\mu}k^{\mu} + \dots \quad (1.58)$$

where $C(\kappa_{\text{nn}}, k)$ is a sub-polynomial function, which is roughly constant, *i.e.* $C(\kappa_{\text{nn}}, k) \approx C$, and

\dots represents *lower* powers of κ_{nn} and k , that are negligible in the asymptotic limit. In the context of stability the diagonal terms of J_{ij} are assumed to be negative, capturing a stabilizing negative feedback, hence the $-C$ term in (1.58), which is negative if $C > 0$.

We can now piece our results together to construct the complete Jacobian as appears in Eq. (1.5), rewriting it as

$$J_{ij} = A_{ij}W_{ij} + \delta_{ij}D_{ii} = -\delta_{ij}C\kappa_{\text{nn}}^{\xi\mu}k_i^\mu + A_{ij}\kappa_{\text{nn}}^{\xi(\nu+\rho)}k_i^\nu k_j^\rho, \quad (1.59)$$

where the first term on the r.h.s. represents the (negative) diagonal entries, and second term captures the off-diagonal entries, which are non-zero only if $A_{ij} = 1$; δ_{ij} is the Kronecker delta function. As we are only interested in the sign of the principle eigenvalue, but not in its specific magnitude, we have the degree of freedom to multiply J_{ij} by an arbitrary constant. We therefore normalize J_{ij} by $\kappa_{\text{nn}}^{-\xi(\nu+\rho)}$, providing

$$J_{ii} \sim -C\kappa_{\text{nn}}^\eta k_i^\mu \quad (1.60)$$

$$J_{ij} \sim A_{ij}k_i^\nu k_j^\rho \quad (1.61)$$

for the diagonal and off-diagonal terms respectively, with $\eta = \xi(\mu - \nu - \rho)$ - recovering Eqs. (7) and (8) of the main text.

Equations (1.60) and (1.61) describe the asymptotic structure of the diagonal and off-diagonal Jacobian terms, as extracted from the general dynamics of Eq. (1.1). The resulting J_{ij} is characterized by several distinct structural and dynamic inputs: A_{ij} , the network topology, which determines the non-vanishing off-diagonal elements. It also determines the degrees k_i, k_j and the average neighbor degree κ_{nn} . The exponents

$$\Omega = (\eta, \mu, \nu, \rho) \quad (1.62)$$

are fully independent of the network topology, extracted from the dynamic functions $M_0(x), M_1(x)$ and $M_2(x)$, *i.e.* the interaction mechanisms driving Eq. (1.1). These exponents are universal in the sense that they do not depend of the specific model *parameters*, but rather on the *model* itself, *e.g.*, Social, Regulatory etc. The coefficient C , in contrast, is non-universal, and its value is determined by the specific rate-constants and time-scales driving Eq. (1.1); here we do not attempt to predict the magnitude of this coefficient. In the limit of sufficiently large k_i and k_j , and, where applicable - in the limit of large κ_{nn} , the specific finite value of C has negligible impact on the principle eigenvalue of J_{ij} as we explicitly show in Sec. 3. Hence stability is asymptotically determined by the exponents Ω , independent of C . The meaning is that the *model* can be asymptotically stable or unstable, regardless of its specific *parameters*.

1.4.1 Impact of $P(k)$ and κ_{nn}

In this derivation we considered only the *scaling* of J_{ij} on the degrees k_i, k_j , and on the nearest neighbor degree κ_{nn} . We disregarded coefficients, such as C_n or G_n in (1.41) and (1.31), or sub-polynomial functions like $f(k)$ in (1.17). The rationale is that in the limit of large degrees the Jacobian spectrum is mainly impacted by these asymptotic scaling relationships, and has little dependence on finite size coefficients that do not scale with k, κ_{nn} , and hence also do not grow

significantly as a function of system size N . Indeed, May's paradox is rooted precisely in such scaling, in which the principle eigenvalue grows asymptotically as $\sim N^c$ (in May's work $c = 1/2$) rendering stability independent of finite coefficients, such as the system's intrinsic time-scales⁷. Therefore, Eqs. (1.60) and (1.61) are especially relevant when $P(k)$ is fat-tailed, *e.g.*, scale-free, where the hub-degrees and the nearest neighbor degree can potentially scale with N .

The role of κ_{nn} . While k_i is a node specific attribute, that captures a specific dependency between the i th diagonal term and i 's degree, the pre-factor κ_{nn}^η represents a network aggregated parameter, indeed - a *constant*, whose impact is often negligible in the asymptotic limit of large k . We include it in our analysis, however, because under extreme degree-heterogeneity, we may observe that κ_{nn} diverges as $\kappa_{\text{nn}} \sim N^\beta$ (1.25), and therefore *can* potentially impact the system stability under $N \rightarrow \infty$. For example, in a scale-free network where $P(k) \sim k^{-\gamma}$, we can use $\kappa_{\text{nn}} = \langle k^2 \rangle / \langle k \rangle$ in (1.23) to obtain

$$\kappa_{\text{nn}} \sim \begin{cases} N & \gamma < 2 \\ N^{3-\gamma} & 2 \leq \gamma < 3 \\ \log(N) & \gamma \geq 3 \end{cases}, \quad (1.63)$$

which scales with N as long as $\gamma < 3$. There are, however, broad conditions, that arise quite naturally in many real systems, in which the κ_{nn} term in (1.60) can be neglected, significantly simplifying the stability analysis:

- **Finite κ_{nn} .** In case $\gamma \geq 3$, κ_{nn} no longer scales with N , it behaves as a constant and has no impact in the asymptotic limit. Under these conditions it suffices to write Eq. (1.60) as $J_{ii} \sim -Ck_i^\mu$.
- **Bounded activities.** In some models the activities x_i are bounded. For example, in spreading processes, from epidemics to cascading failures, the activities satisfy $0 \leq x_i \leq 1$. Under these conditions the leading power in the power-series expansion of (1.18) is zero, and hence $x(k \rightarrow \infty) \sim 1$. The result is that the nearest neighbor activity x_{nn} , associated with degree κ_{nn} is itself bounded, and even if $\kappa_{\text{nn}} \rightarrow \infty$ *à la* Eq. (1.63), we still have $x_{\text{nn}} \sim 1$. Consequently $M_2(x_{\text{nn}})$ in (1.30) also approaches a constant value, and therefore the leading power in the expansion (1.31) is $\Psi(0) = 0$. This provides, based on Eq. (1.33), $\xi = 0$, which in turn leads to $\eta = 0$ in (1.60), again resulting in $J_{ii} \sim -Ck_i^\mu$, independent of κ_{nn} .
- **Saturating $M_2(x)$.** Another common feature in many relevant models is that $M_2(x_j \rightarrow \infty) \rightarrow 1$. This represents the saturating impact of node j on its nearest neighbor i , as frequently observed in regulatory processes or in population dynamics. Once again, we have $M_2(x_{\text{nn}}) \sim 1$, providing $\xi = 0$, and consequently $\eta = 0$ in (1.60).

The ensemble $\mathbb{E}(A_{ij}, \Omega)$ summary

Starting from Eq. (1.1) we use $M_0(x)$, $M_1(x)$ and $M_2(x)$ to construct the functions

$$R(x) = -\frac{M_1(x)}{M_0(x)}, \quad Y(x) = M_1(x)R'(x), \quad Z(x) = R(x)M_2(x). \quad (1.64)$$

From these we extract the four relevant power-series expansions

$$\begin{aligned} M_2(Z^{-1}(x)) &= \sum_{n=0}^{\infty} G_n x^{\Psi(n)}, & Y(R^{-1}(x)) &= \sum_{n=0}^{\infty} C_n x^{\Gamma(n)}, \\ M_1(R^{-1}(x)) &= \sum_{n=0}^{\infty} K_n x^{\Pi(n)}, & M_2'(R^{-1}(x)) &= \sum_{n=0}^{\infty} L_n x^{\Theta(n)} \end{aligned} \quad (1.65)$$

whose leading powers determine the dynamic exponents $\Omega = (\eta, \mu, \nu, \rho)$ as

$$\mu = 2 - \Gamma(0), \quad \nu = -\Pi(0), \quad \rho = -\Theta(0), \quad \eta = -\Psi(0)(\mu - \nu - \rho). \quad (1.66)$$

To construct $J_{ij} \in \mathbb{E}(A_{ij}, \Omega)$ we first generate the network A_{ij} , then extract the degrees k_i of all nodes and the nearest neighbor degree κ_{nn} from Eq. (1.22). The resulting J_{ij} satisfies

$$J_{ii} \sim -C \kappa_{\text{nn}}^{\eta} k_i^{\mu} \quad (1.67)$$

$$J_{ij} \sim A_{ij} k_i^{\nu} k_j^{\rho}, \quad (1.68)$$

where the constant $C > 0$ is arbitrary.

2 Analyzing the dynamic models

To demonstrate our formalism we examined several commonly used dynamic models, as listed in Fig. 1g of the main text. Below we extract the exponents Ω for each of these models.

2.1 Social dynamics

As an example of Social dynamics we used epidemic spreading via the Susceptible-Infected-Susceptible (SIS) model, in which $x_i(t)$ captures the probability of infection of node i . Denoting the susceptible state by S and the infected state by I , the model includes the following transitions



capturing the processes of recovery at a rate f and infection at rate g . This gives rise to the dynamic equation⁸

$$\frac{dx_i}{dt} = -fx_i + \sum_{j=1}^N A_{ij}g(1-x_i)x_j, \quad (2.3)$$

characterized by the dynamic functions $M_0(x) = -fx$, $M_1(x) = 1 - x$ and $M_2(x) = gx$.

To obtain the relevant J_{ij} ensemble, we seek the exponents $\Omega = (\eta, \mu, \nu, \rho)$. We begin by translating the given functions $M_0(x), M_1(x), M_2(x)$ in to the relevant functions shown in (1.64), providing

$$R(x) = -\frac{M_1(x)}{M_0(x)} = \frac{1-x}{fx} \quad (2.4)$$

$$Y(x) = M_1(x)R'(x) = \frac{x-1}{fx^2} \quad (2.5)$$

$$Z(x) = R(x)M_2(x) = \frac{g}{f} - \frac{g}{f}x. \quad (2.6)$$

Inverting $R(x)$ and $Z(x)$, we write

$$R^{-1}(x) = \frac{1}{fx+1}, \quad (2.7)$$

$$Z^{-1}(x) = 1 - \frac{f}{g}x, \quad (2.8)$$

allowing us to construct the Hahn expansions of (1.65) as

$$M_2(Z^{-1}(x)) = gZ^{-1}(x) = g - fx \quad (2.9)$$

$$Y(R^{-1}(x)) = \frac{R^{-1}(x) - 1}{f \times (R^{-1}(x))^2} = -x - fx^2 \quad (2.10)$$

$$M_1(R^{-1}(x)) = 1 - R^{-1}(x) = \frac{fx}{fx + 1} = fx - f^2x^2 + f^3x^3 - \dots \quad (2.11)$$

$$M_2'(R^{-1}(x)) = g. \quad (2.12)$$

Each of these functions is expressed as a Hahn power-series, in some cases a finite polynomial, *e.g.*, (2.9) or (2.10), and in others an infinite series, where we only write the leading terms around $x \rightarrow 0$. Here, coincidentally, the last function (2.12) is a constant, with the only power being x^0 . We can list the relevant powers in these Hahn expansions as $\Psi(0) = 0, \Gamma(0) = 1, \Pi(0) = 1$ and $\Theta(0) = 0$, which, using (1.66) provides

$$\mu = 2 - \Gamma(0) = 1 \quad (2.13)$$

$$\nu = -\Pi(0) = -1 \quad (2.14)$$

$$\rho = -\Theta(0) = 0 \quad (2.15)$$

$$\eta = -\Psi(0)(\mu - \nu - \rho) = 0. \quad (2.16)$$

2.2 Regulatory dynamics

We used the Michaelis-Menten model to capture gene Regulatory dynamics⁹. Here, Eq. (1.1) tracks the level of gene expression $x_i(t)$, as regulated via the sub-cellular network A_{ij} , providing

$$\frac{dx_i}{dt} = -Bx_i^a + \sum_{j=1}^N A_{ij} \frac{x_j^h}{1 + x_j^h}. \quad (2.17)$$

The self-dynamic term $M_0(x) = -Bx^a$ captures biochemical processes¹⁰, such as degradation ($a = 1$) or dimerization ($a = 2$). The interaction terms $M_1(x) = 1, M_2(x) = x^h/1 + x^h$ describe genetic activation, a switch-like dynamics, which ranges from $M_2(0) = 0$ to $M_2(x \rightarrow \infty) = 1$ to capture activation of gene i by gene j . The Hill coefficient h governs the rate of saturation of $M_2(x)$.

First, we construct the three functions summarized in (1.64):

$$R(x) = -\frac{M_1(x)}{M_0(x)} = \frac{1}{Bx^a} \quad (2.18)$$

$$Y(x) = M_1(x)R'(x) = -\frac{a}{Bx^{a+1}} \quad (2.19)$$

$$Z(x) = R(x)M_2(x) = \frac{x^h}{B(x^a + x^{a+h})}. \quad (2.20)$$

Inverting $R(x)$, we write

$$R^{-1}(x) = B^{-\frac{1}{a}} x^{-\frac{1}{a}}, \quad (2.21)$$

allowing us to construct the Hahn expansions (1.65)

$$Y(R^{-1}(x)) = -\frac{a}{B} \left(\frac{1}{Bx} \right)^{-\frac{a+1}{a}} = aB^{\frac{1}{a}} x^{\frac{a+1}{a}} \quad (2.22)$$

$$M_1(R^{-1}(x)) = 1 = x^0 \quad (2.23)$$

$$M_2'(R^{-1}(x)) = \frac{hB^{-\frac{h-1}{a}} x^{-\frac{h-1}{a}}}{\left(1 + B^{-\frac{h}{a}} x^{-\frac{h}{a}}\right)^2} = hB^{\frac{h+1}{a}} x^{\frac{h+1}{a}} - 2hB^{\frac{2h+1}{a}} x^{\frac{2h+1}{a}} + \dots \quad (2.24)$$

In each of these expansions we write the leading terms in the $x \rightarrow 0$ limit: in (2.22) and (2.23) the expansion features a single term, *i.e.* a pure monomial, and in (2.24) we show the first two terms of the relevant Hahn expansion. To obtain Ω we extract only the leading *powers* $\Gamma(0) = (a+1)/a$, $\Pi(0) = 0$, $\Theta(0) = (h+1)/a$, ignoring the *coefficients*, *e.g.*, $aB^{1/a}$ or $hB^{(h+1)/a}$. We can now use (1.66) to extract the dynamic exponents as

$$\mu = 2 - \Gamma(0) = \frac{a-1}{a} \quad (2.25)$$

$$\nu = -\Pi(0) = 0 \quad (2.26)$$

$$\rho = -\Theta(0) = -\frac{h+1}{a}. \quad (2.27)$$

To obtain η we must calculate $M_2(Z^{-1}(x))$, requiring us to invert the function $Z(x)$ in (2.20), which becomes analytically prohibitive for general a and h . Fortunately, in Regulatory dynamics we can calculate this term directly. We first recall, from Eq. (1.30) that $M_2(Z^{-1}(q_{\odot})) = M_2(x_{\text{nn}})$, where x_{nn} is the average neighbor activity and $q_{\odot} \sim 1/\kappa_{\text{nn}}$ is the average neighbor degree. For a general node with degree k we can use (1.18) together with (2.21) to write

$$x(k) = B^{-\frac{1}{a}} q^{-\frac{1}{a}} \sim k^{\frac{1}{a}}, \quad (2.28)$$

a positive scaling with k , predicting that $x(k \rightarrow \infty) \rightarrow \infty$, namely that a node's activity increases with its degree. Consequently, under a sufficiently large κ_{nn} , the nearest neighbor activity x_{nn} also diverges as $\kappa_{\text{nn}}^{1/a}$, or alternatively, as $q_{\odot}^{-1/a}$. Hence we write

$$M_2(x_{\text{nn}}) = \frac{x_{\text{nn}}^h}{1 + x_{\text{nn}}^h} \sim \frac{q_{\odot}^{-\frac{h}{a}}}{1 + q_{\odot}^{-\frac{h}{a}}} = \frac{1}{1 + q_{\odot}^{\frac{h}{a}}} = 1 - q_{\odot}^{\frac{h}{a}} + \dots, \quad (2.29)$$

observing directly that the leading power of $M_2(x_{\text{nn}})$, and therefore also of $M_2(Z^{-1}(x))$ is $\Psi(0) = 0$. As a result, we obtain, using (1.66) our final exponent

$$\eta = -\Psi(0)(\mu - \nu - \rho) = 0. \quad (2.30)$$

This is, in fact, precisely the case of *Bounded* $M_2(x)$, discussed in Sec. 1.4.1, for which we *a priori* predicted $\eta = 0$.

2.3 Ecological dynamics

We consider mutualistic eco-systems, such as plant-pollinator networks, in which the interacting species exhibit symbiotic relationships. The species populations follow the dynamic equation

$$\frac{dx_i}{dt} = Bx_i(t) \left(1 - \frac{x_i(t)}{K}\right) + \sum_{j=1}^N A_{ij}x_i(t)F(x_j(t)). \quad (2.31)$$

The self dynamics

$$M_0(x) = Bx \left(1 - \frac{x}{K}\right) \quad (2.32)$$

captures logistic growth: when the population is small, the species reproduce at a rate B , yet, as x_i approaches the carrying capacity of the system K , growth is hindered by competition over limited resources¹¹. The mutualistic inter-species interactions are captured by $M_1(x) = x$ and $M_2(x) = F(x)$, where $F(x)$ represents the *functional response*, describing the positive impact that species j has on species i . This functional response can take one of several forms¹²:

Type slowromancapi@: linear impact

$$F(x) = x. \quad (2.33)$$

Type slowromancapii@: saturating impact

$$F(x) = \frac{x}{1+x}. \quad (2.34)$$

Type slowromancapiiii@: a generalization of Type slowromancapii@, where

$$F(x) = \frac{x^h}{1+x^h}. \quad (2.35)$$

In our simulations we used Type slowromancapii@ mutualistic interactions, therefore

$$M_2(x) = \frac{x}{1+x}. \quad (2.36)$$

For simplicity, we set the coefficients to $B = K = 1$.

For $R(x)$, $Y(x)$ and $Z(x)$ we have

$$R(x) = -\frac{M_1(x)}{M_0(x)} = \frac{1}{x-1} \quad (2.37)$$

$$Y(x) = M_1(x)R'(x) = -\frac{x}{(x-1)^2} \quad (2.38)$$

$$Z(x) = R(x)M_2(x) = \frac{x}{x^2-1}. \quad (2.39)$$

Inverting $R(x)$ and $Z(x)$, we write

 Social	$\frac{dx_i}{dt} = -fx_i + \sum_{j=1}^N A_{ij}g(1-x_i)x_j$	$\Omega = (0, 1, -1, 0)$	$S = -\beta$
 Regulatory	$\frac{dx_i}{dt} = -Bx_i^a + \sum_{j=1}^N A_{ij} \frac{x_j^h}{1+x_j^h}$	$\Omega = \left(0, \frac{a-1}{a}, 0, -\frac{h+1}{a}\right)$	$S = -\frac{h}{a}\beta$
 Ecological	$\frac{dx_i}{dt} = Bx_i \left(1 - \frac{x_i}{K}\right) + \sum_{j=1}^N A_{ij}x_i \frac{x_j}{1-x_j}$	$\Omega = (0, 1, 1, -2)$	$S = -\beta$
 Biochemical	$\frac{dx_i}{dt} = F - Wx_i - \tilde{B} \sum_{j=1}^N A_{ij}x_i x_j$	$\Omega = (-1, 1, -1, 0)$	$S_{\text{Neg}} = -\beta$

Figure 6: **Dynamic models - summary.** Our four dynamic models and their associated exponents Ω . For each model we also show the stability classifier S . For Biochemical we use S_{Neg} , see Sec. 3.2

$$R^{-1}(x) = \frac{x+1}{x}, \quad (2.40)$$

$$Z^{-1}(x) = \frac{1}{2x} \left(1 + \sqrt{1+4x^2}\right), \quad (2.41)$$

where in $Z^{-1}(x)$ we choose the positive solution, corresponding to the non-zero fixed-point of (2.31). Next, we construct the Hahn expansions of (1.65) as

$$M_2(Z^{-1}(x)) = \frac{Z^{-1}(x)}{1+Z^{-1}(x)} = \frac{1+\sqrt{1+4x^2}}{2x+1+\sqrt{1+4x^2}} = 1-x+\dots \quad (2.42)$$

$$Y(R^{-1}(x)) = -\frac{R^{-1}(x)}{(R^{-1}(x)-1)^2} = x+x^2 \quad (2.43)$$

$$M_1(R^{-1}(x)) = \frac{x+1}{x} = x^{-1}+1 \quad (2.44)$$

$$M'_2(R^{-1}(x)) = \frac{1}{(R^{-1}(x)+1)^2} = \frac{x^2}{4x^2+4x+1} = x^2-4x^3+\dots, \quad (2.45)$$

whose leading powers are $\Psi(0) = 0, \Gamma(0) = 1, \Pi(0) = -1$ and $\Theta(0) = 2$. Consequently, the dynamic exponents in (1.66) are

$$\mu = 2 - \Gamma(0) = 1 \quad (2.46)$$

$$\nu = -\Pi(0) = 1 \quad (2.47)$$

$$\rho = -\Theta(0) = -2 \quad (2.48)$$

$$\eta = -\Psi(0)(\mu - \nu - \rho) = 0, \quad (2.49)$$

once again, predicting $\eta = 0$, this time thanks both to the *Bounded activities* ($0 < x_i < K$) and to the *Saturating* nature of the interaction function $M_2(x)$ (Sec. 1.4.1).

2.4 Biochemical dynamics

As a Biochemical model we consider protein-protein interactions (PPI), which are driven by three processes: $\phi \rightarrow P_i$, describing the synthesis of the i th protein P_i at a rate F ; $P_i \rightarrow \phi$, describing protein degradation at rate W ; $P_i + P_j \rightleftharpoons P_i P_j$ describing the binding and unbinding of a pair of interacting proteins at rates B and U respectively. The hetero-dimer $P_i P_j$ undergoes degradation $P_i P_j \rightarrow \phi$ at rate Q . The dynamical equations for this system are^{10,13}

$$\frac{dx_i}{dt} = F - Wx_i(t) + \sum_{j=1}^N Ux_{ij}(t) - B \sum_{j=1}^N A_{ij}x_i(t)x_j(t) \quad (2.50)$$

$$\frac{dx_{ij}}{dt} = BA_{ij}x_i(t)x_j(t) - (U + Q)x_{ij}(t), \quad (2.51)$$

where $x_i(t)$ is the concentration of P_i and $x_{ij}(t)$ is the concentration of the hetero-dimer $P_i P_j$. Under time-scale separation we assume that the hetero-dimer concentration is at steady-state, setting $dx_{ij}/dt = 0$ in (2.51). This provides us with

$$\frac{dx_i}{dt} = F - Wx_i(t) - \tilde{B} \sum_{j=1}^N A_{ij}x_i(t)x_j(t), \quad (2.52)$$

where the effective binding rate is $\tilde{B} = QB/(U + Q)$. Hence, in the effective equation (2.52) we have $M_0(x) = F - Wx$, $M_1(x) = -\tilde{B}x$ and $M_2(x) = x$, providing the dynamic functions (1.64)

$$R(x) = -\frac{M_1(x)}{M_0(x)} = \frac{\tilde{B}x}{F - Wx} \quad (2.53)$$

$$Y(x) = M_1(x)R'(x) = -\frac{F\tilde{B}^2x}{(F - Wx)^2} \quad (2.54)$$

$$Z(x) = R(x)M_2(x) = \frac{\tilde{B}x^2}{F - Wx}. \quad (2.55)$$

The inverse functions are, therefore

$$R^{-1}(x) = \frac{Fx}{\tilde{B} + Wx} \quad (2.56)$$

$$Z^{-1}(x) = \frac{W}{2\tilde{B}}x \left(-1 + \sqrt{1 + \frac{4\tilde{B}F}{W^2x}} \right), \quad (2.57)$$

where in $Z^{-1}(x)$ we choose the positive solution, corresponding to the positive fixed-point of (2.52). We can now compose the functions in (1.65), obtaining

$$M_2(Z^{-1}(x)) = Z^{-1}(x) = \sqrt{\frac{F}{\tilde{B}}}x^{\frac{1}{2}} + \frac{W^2}{8\tilde{B}^2F^{\frac{1}{2}}}x^{\frac{3}{2}} + \dots \quad (2.58)$$

$$Y(R^{-1}(x)) = -\frac{F\tilde{B}^2R^{-1}(x)}{(F - WR^{-1}(x))^2} = F\tilde{B}^2x + F\tilde{B}Wx^2 \quad (2.59)$$

$$M_1(R^{-1}(x)) = -\frac{\tilde{B}Fx}{\tilde{B} + Wx} = -Fx + \frac{FW}{\tilde{B}}x^2 + \dots \quad (2.60)$$

$$M_2'(R^{-1}(x)) = 1, \quad (2.61)$$

allowing us to extract the leading powers as $\Psi(0) = 1/2, \Gamma(0) = 1, \Pi(0) = 1$ and $\Theta(0) = 0$. These powers provide the dynamic exponents via (1.66), providing, for Biochemical

$$\mu = 2 - \Gamma(0) = 1 \quad (2.62)$$

$$\nu = -\Pi(0) = -1 \quad (2.63)$$

$$\rho = -\Theta(0) = 0 \quad (2.64)$$

$$\eta = -\Psi(0)(\mu - \nu - \rho) = -1. \quad (2.65)$$

3 Principle eigenvalue of $J_{ij} \in \mathbb{E}(A_{ij}, \Omega)$

The stability of Eq. (1.1) can be characterized by the principal eigenvalue λ of J_{ij} in (1.67) - (1.68). As the entries depend on k_i and k_j , the value of λ is driven by the limit of large k - specifically, in a degree-heterogeneous network, it is determined by the nearest neighbor degree κ_{nn} , which can potentially diverge with the system size N as

$$\kappa_{nn} \sim N^\beta. \quad (3.1)$$

As opposed to the *dynamic* exponents Ω , the exponent β is a *topological* exponent, determined by the network's degree distribution $P(k)$. In a scale-free network, for example β is extracted from (1.63).

To approximate this hub-periphery structure, we use a *star* network, in which a single hub is linked to

$$k = \kappa_{nn} \sim N^\beta \quad (3.2)$$

peripheral nodes. This captures the environment of a typical hub in, *e.g.*, a scale-free network. Indeed, the hubs in a scale-free network can be viewed as a collection of weakly coupled *stars*, that are only sparsely linked to each other¹⁴. Under these conditions we have the $(k+1) \times (k+1)$

network

$$A_{ij} = \begin{bmatrix} 0 & 1 & 1 & \dots & 1 \\ 1 & 0 & 0 & \dots & 0 \\ \vdots & & \ddots & & \vdots \\ 1 & 0 & 0 & \dots & 0 \end{bmatrix}, \quad (3.3)$$

which using (1.67) and (1.68), provides the corresponding Jacobian as

$$J_{ij} = -C\tilde{\kappa}_{\text{nn}}^\eta \begin{bmatrix} k^\mu & 0 & \dots & 0 \\ 0 & 1 & \dots & 0 \\ \vdots & & \ddots & \vdots \\ 0 & 0 & \dots & 1 \end{bmatrix} + \begin{bmatrix} 0 & k^\nu & \dots & k^\nu \\ k^\rho & 0 & \dots & 0 \\ \vdots & & \ddots & \vdots \\ k^\rho & 0 & \dots & 0 \end{bmatrix}, \quad (3.4)$$

where $C > 0$. In (3.4) we used $\tilde{\kappa}_{\text{nn}}$ to express the nearest neighbor degree in our star construction, which is potentially distinct from κ_{nn} of the originally approximated scale-free network. Lacking an *a priori* estimate for this parameter we express it as

$$\tilde{\kappa}_{\text{nn}} \sim N^\alpha, \quad (3.5)$$

leaving us a degree of freedom to later tune α such that the prediction from our star construction best captures the observed results from a real scale-free network. Hence, β , characterizing the star-hub (k), is extracted from A_{ij} via (3.1) and α is a tunable parameter, which we select for the star-model to best fit the complete scale-free network results.

We emphasize that the star approximation in (3.3) by no means captures the complete behavior of a real scale-free network, as indeed it represents but a crude representation of an isolated hub environment. However, our goal here is to examine stability vs. instability - a feature that only depends on the *sign* of the principal eigenvalue, not on its specific value, and is, therefore, insensitive to the detailed structure of A_{ij} . As we show in Fig. 4 of the main text, the star approximation, while highly stylized, is, indeed, sufficient to capture this J_{ij} characteristic.

To obtain the principal eigenvalue we solve the linear equation

$$J\mathbf{v} = \lambda\mathbf{v}. \quad (3.6)$$

Using the symmetry of (3.4), we seek a solution of the form $\mathbf{v} = (a, b, b, \dots, b)^\top$, allowing us to reduce (3.6) into

$$-C\tilde{\kappa}_{\text{nn}}^\eta k^\mu a + k k^\nu b = \lambda a \quad (3.7)$$

$$k^\rho a - C\tilde{\kappa}_{\text{nn}}^\eta b = \lambda b. \quad (3.8)$$

Note that in \mathbf{v} the specific values of a, b have no significance, only the ratio a/b , as we are only interested in the *direction* of the eigenvector, not its magnitude. We therefore arbitrarily set $a = 1$, allowing us to solve (3.7) - (3.8) and obtain

$$\lambda = \frac{1}{2} \left(-C\tilde{\kappa}_{\text{nn}}^\eta (k^\mu + 1) + \sqrt{C^2\tilde{\kappa}_{\text{nn}}^{2\eta} (k^\mu + 1)^2 - 4C^2\tilde{\kappa}_{\text{nn}}^{2\eta} k^\mu + 4k^{1+\nu+\rho}} \right), \quad (3.9)$$

where, of the two solutions, we selected only the one in which the square-root is added (rather than subtracted), as we seek the *largest* eigenvalue. Seeking the limit

$$\lim_{N \rightarrow \infty} (\lambda), \quad (3.10)$$

we use (3.2) and (3.5) to rewrite (3.9) as

$$\begin{aligned} \lambda \sim & \frac{1}{2} \left(-CN^{\alpha\eta} (N^{\beta\mu} + 1) \right. \\ & \left. + \sqrt{C^2 N^{2\alpha\eta} (N^{\beta\mu} + 1)^2 + 4 [-C^2 N^{2\alpha\eta+\beta\mu} + N^{\beta(1+\nu+\rho)}]} \right), \end{aligned} \quad (3.11)$$

in which we replace $\tilde{\kappa}_{\text{nn}}$ and k by N^α and N^β , respectively. In (3.11) we ignore the pre-factors of the N -scaling, focusing only on the powers (α, β) , hence substituting the equality sign $=$ with the asymptotic scaling operator \sim .

The case where $\mu > 0$. First we analyze λ under $\mu > 0$. Here, we write $N^{\beta\mu} \gg 1$, simplifying (3.11) in the limit $N \rightarrow \infty$ into

$$\lambda \sim \frac{1}{2} \left(-CN^{\alpha\eta+\beta\mu} + \sqrt{C^2 N^{2(\alpha\eta+\beta\mu)} + 4 [-C^2 N^{2\alpha\eta+\beta\mu} + N^{\beta(1+\nu+\rho)}]} \right). \quad (3.12)$$

Extracting the common terms out of the product we rewrite (3.12) as

$$\lambda \sim \frac{1}{2} CN^{\alpha\eta+\beta\mu} \left(-1 + \sqrt{1 + 4 \left(-N^{-\beta\mu} + \frac{1}{C^2} N^\sigma \right)} \right), \quad (3.13)$$

where

$$\sigma = \beta \left(1 + \nu + \rho - 2\mu - 2\frac{\alpha}{\beta}\eta \right). \quad (3.14)$$

Note that $N^{-\beta\mu} \leq 1$ in (3.13), as $\mu > 0$. Therefore, in case $\sigma \geq 0$, the N^σ term dominates the r.h.s. of the equation, providing, under $N \rightarrow \infty$,

$$\lambda \sim \frac{C}{\sqrt{C^2}} N^{\frac{1}{2}\sigma + \alpha\eta + \beta\mu}, \quad (3.15)$$

which, since $C > 0$ is guaranteed to be positive, *i.e.* the system is *unstable*.

Next we consider the case $\sigma < 0$. Under these conditions $N^\sigma \ll 1$, allowing us to expand the square-root in (3.13) to first order, providing

$$\lambda \sim \frac{1}{2} CN^{\alpha\eta+\beta\mu} \left(-1 + 1 + 2 \left(-N^{-\beta\mu} + \frac{1}{C^2} N^\sigma \right) \right) = -CN^{\alpha\eta} + \frac{1}{C} N^{\sigma + \alpha\eta + \beta\mu}. \quad (3.16)$$

We can rewrite this in the form of Eq. (9) of the main text, obtaining

$$\lambda \sim N^Q \left(1 - \frac{C}{N^S} \right), \quad (3.17)$$

where

$$Q = \sigma + \alpha\eta + \beta\mu \quad (3.18)$$

$$S = \sigma + \beta\mu. \quad (3.19)$$

As N^Q is guaranteed to be positive, the sign of λ depends on S : in case $S > 0$ the negative term in (3.17) satisfies $CN^{-S} \ll 1$, and hence we have $\lambda \sim N^Q > 0$, an unstable dynamics. If however $S < 0$, we have $-CN^{-S} \rightarrow -\infty$, predicting $\lambda < 0$, regardless of C , an asymptotically stable system. Consequently the system is stable as long as $S < 0$, which using (3.19), and taking σ from (3.14), predicts the stability condition

$$\beta \left(1 + \nu + \rho - \mu - 2\frac{\alpha}{\beta}\eta \right) < 0. \quad (3.20)$$

This condition reduces stability into a small set of *relevant* parameters: β , characterizing the network topology A_{ij} , and $\Omega = (\eta, \mu, \nu, \rho)$, associated with the dynamics $M_0(x), M_1(x), M_2(x)$. The non-universal parameter C becomes irrelevant in the limit of sufficiently large N . Finally, α can be selected to tune the star approximation optimally to the case of a real scale-free A_{ij} , as we do below. Note that condition (3.20) can also be expressed as $\sigma + \beta\mu < 0$. This implies that if $\sigma > \beta\mu$ the system is unstable. This instability condition already contains the previously obtained condition of $\sigma > 0$, that led to Eq. (3.15). Therefore, Eq. (3.20) is sufficient to characterize the system's stability.

Finally, the case $S = 0$ in (3.17) represents sensitive stability, in which λ 's value is not asymptotically defined, and rather it depends on the coefficient C . In this class, stability is no longer a characteristic of the dynamic *model*, but rather of its specific rate constants, as encapsulated within C . A trivial example is when $\beta = 0$, *i.e.* a non fat-tailed $P(k)$, for example - Erdős-Rényi. Indeed, as we discuss in the main text, in such networks, stability can be tuned by the model parameters, lacking a defined asymptotic behavior.

The case where $\mu \leq 0$. Here, we have $N^{\beta\mu} \leq 1$, and hence Eq. (3.11) can be approximated by

$$\lambda \sim \frac{1}{2} \left(-CN^{\alpha\eta} + \sqrt{C^2 N^{2\alpha\eta} + 4[-C^2 N^{2\alpha\eta + \beta\mu} + N^{\beta(1+\nu+\rho)}]} \right), \quad (3.21)$$

leading to

$$\lambda \sim \frac{1}{2} CN^{\alpha\eta} \left(-1 + \sqrt{1 + 4 \left(-N^{\beta\mu} + \frac{1}{C^2} N^\omega \right)} \right), \quad (3.22)$$

where

$$\omega = \beta \left(1 + \nu + \rho - 2\frac{\alpha}{\beta}\eta \right). \quad (3.23)$$

Once again, we have $N^{\beta\mu} \leq 1$, this time since $\mu < 0$. Therefore, as before, if $\omega > 0$, λ becomes dominated by the N^ω term, following

$$\lambda \sim \frac{C}{\sqrt{C^2}} N^{\frac{1}{2}\omega + \alpha\eta}, \quad (3.24)$$

which is always positive, *i.e. unstable*. If, however, $\omega < 0$, we use a linear approximation to write

$$\lambda \sim \frac{1}{2} C N^{\alpha\eta} \left(-1 + 1 + 2 \left(-N^{\beta\mu} + \frac{1}{C^2} N^\omega \right) \right) = -C N^{\alpha\eta + \beta\mu} + \frac{1}{C} N^{\omega + \alpha\eta}, \quad (3.25)$$

once again - a competition between a positive vs. a negative term. Collecting the powers we, again, rewrite (3.25) in the form

$$\lambda \sim N^Q \left(1 - \frac{C}{N^S} \right), \quad (3.26)$$

where this time

$$Q = \omega + \alpha\eta \quad (3.27)$$

$$S = \omega - \beta\mu. \quad (3.28)$$

Stability is ensured if, for $N \rightarrow \infty$, the negative term dominates, namely if $S < 0$. Using (3.23) to express ω this provides

$$\beta \left(1 + \nu + \rho - \mu - 2 \frac{\alpha}{\beta} \eta \right) < 0, \quad (3.29)$$

recovering precisely the condition in (3.20).

Tuning α . The parameter α represents a degree of freedom, rooted in the fact that the star approximation captures an inaccurate depiction of a real scale-free network. This approximation can be optimized if we select α such that the star best captures the complete scale-free network environment. We find that setting

$$\alpha = \frac{\beta}{2} \quad (3.30)$$

provides the optimal approximation, accurately predicting stability 96% of the time (Fig. 7). This completes the stability analysis, providing the stability classifier as

$$S = \beta (1 + \nu + \rho - \mu - \eta), \quad (3.31)$$

as appears in Eq. (10) of the main text.

3.1 The role of topology vs. dynamics

The stability condition (3.31) is driven by five distinct exponents. The first four exponents $\Omega = (\eta, \mu, \nu, \rho)$ are determined by the dynamic model - Social, Regulatory, Ecological etc. -

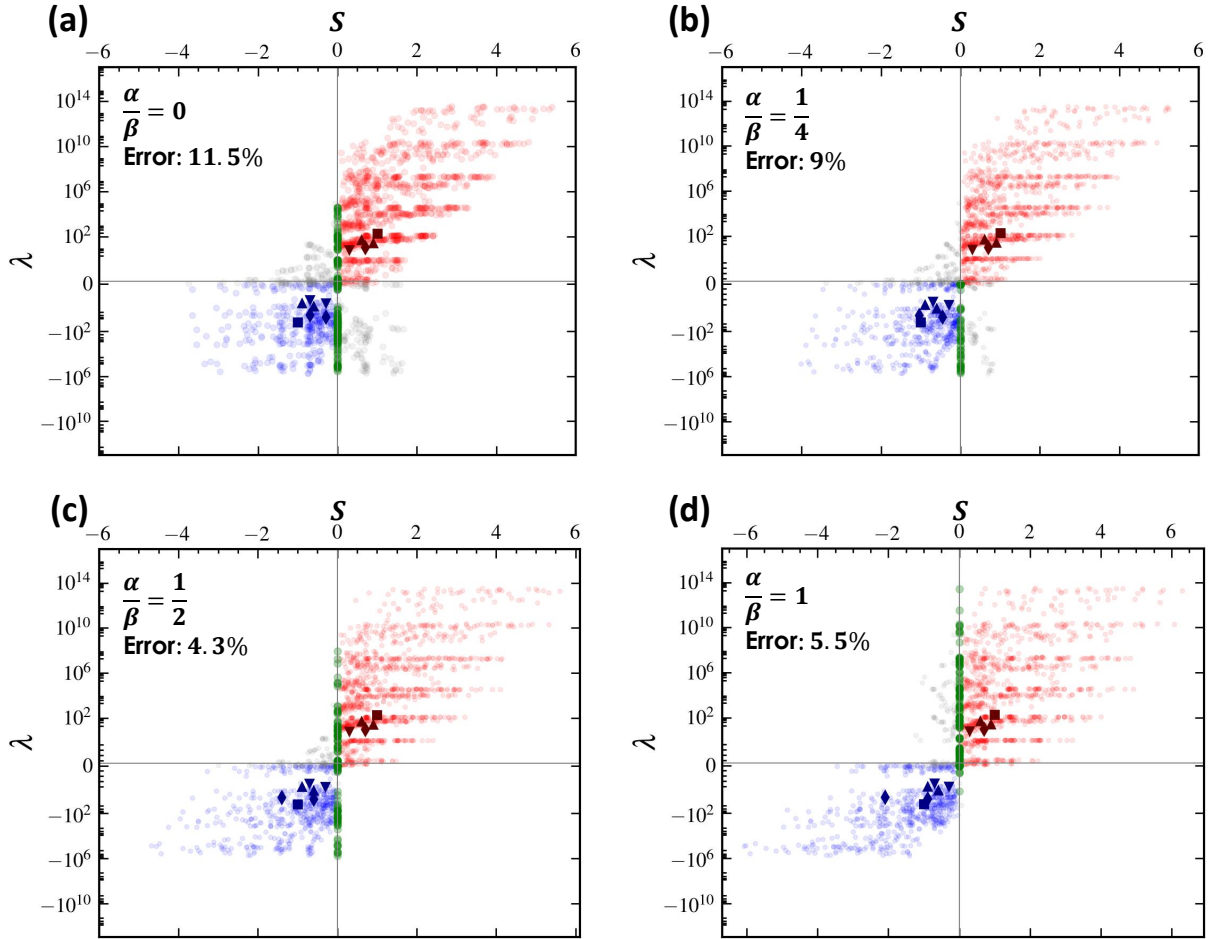


Figure 7: **Tuning the parameter α .** In Eqs. (3.20) and (3.29) we have the degree of freedom to set α/β for the star approximation to best predict the stability of complete scale-free networks. We used our set of 2,077 J matrices (Fig. 4a of main text) to predict stability using different values of α/β . Quantifying the Error by the fraction of mis-classified J matrices (grey dots), we find that setting $\alpha/\beta = 1/2$ provides the optimal fit, securing a $\sim 96\%$ correct classification (Error= 4.3%).

intrinsic to the system's inherent interaction mechanisms. These exponents are independent of the topology A_{ij} or of microscopic model parameters, encapsulated within C , and are therefore *hardwired* into the system's dynamic behavior. For example, our formalism predicts that the SIS model (Social) has $\Omega = (0, 1, -1, 0)$ (Sec. 2.1). This prediction is characteristic of the SIS model, namely it is an intrinsic feature of the SIS interaction mechanisms of infection and recovery. It is, therefore, insensitive to the specific rates of the model - hence Ω remains unchanged if, *e.g.*, a disease has a high or low infection rate, or if it is transmitted via physical contact or aerosols. These will impact the constant C in (1.67), but will have no impact on the universal scaling. Similarly, Ω is unaffected by A_{ij} . Therefore, regardless of whether the disease spreads along the standard social network (Flu) or via sexual transmission (AIDS), as long as the *mechanism* is SIS (or any other mechanism for that matter) Ω remains the same.

The remaining exponent in (3.31), β , on the other hand, is independent of the dynamics, and determined solely by A_{ij} , specifically by its degree distribution $P(k)$, capturing the divergence of κ_{nn} in the limit of large N . For example, under a scale-free topology, where $P(k) \sim k^{-\gamma}$, we have κ_{nn} following Eq. (1.63), predicting

$$\beta = \begin{cases} 1 & \gamma < 2 \\ 3 - \gamma & 2 \leq \gamma < 3 \\ 0 & \gamma \geq 3 \end{cases} . \quad (3.32)$$

Therefore under $\gamma \geq 3$, we have $\beta = 0$ and stability becomes sensitive to parameters (C). On the other hand, under a scale-free topology ($\gamma < 3$) we observe the asymptotic stability/instability driven by $S \neq 0$.

3.2 Stability classifier S under negative interactions

Our formalism is designed to treat cooperative interactions, in which the interaction term $A_{ij}M_1(x_i)M_2(x_j) > 0$. Strictly speaking, our analysis is not designed to treat adversarial interactions, in which the mean-field derivation of Sec. 1 may fail to capture the complex patterns of all activities $x_i(t)$. Specifically, in the presence of negative interactions the steady-states x_i cannot always be expressed as a single variable function of k_i , as appears in Eq. (1.18). Rather, it also depends on i 's neighborhood, *e.g.*, if the neighborhood has high activities, the adversarial interactions will drive x_i to be small, and vice versa. In certain cases, such as in our Biochemical model, this effect is marginal, all neighborhoods have (roughly) the same activity, and hence our analysis continues to apply. The star approximation, however, cannot distinguish between positive and negative interactions - as the derivation yields an identical outcome in both cases. Indeed, this approximation overlooks the potentially stabilizing effect of the negative off-diagonal terms.

Therefore, for simplicity, to evaluate S under negative interactions we consider a fully connected network of

$$k \sim N^\beta \quad (3.33)$$

nodes, *à la* May's original formulation. This simplification may not allow us to fully evaluate the contribution of A_{ij} , as, indeed, we have replaced the network by a single large clique, however, we are only interested in the stability of the *dynamics*, which remains independent of

this simplifying assumption. With *all* nodes now having degree k , the resulting Jacobian takes the form

$$J_{ij} = -Ck^\eta \begin{bmatrix} k^\mu & 0 & \dots & 0 \\ 0 & k^\mu & \dots & 0 \\ \vdots & & \ddots & \vdots \\ 0 & 0 & \dots & k^\mu \end{bmatrix} - \begin{bmatrix} 0 & k^{\nu+\rho} & \dots & k^{\nu+\rho} \\ k^{\nu+\rho} & 0 & \dots & k^{\nu+\rho} \\ \vdots & & \ddots & \vdots \\ k^{\nu+\rho} & k^{\nu+\rho} & \dots & 0 \end{bmatrix}, \quad (3.34)$$

in which both the diagonal and the off-diagonal terms are preceded by a minus sign.

For a matrix of the form (3.34) the principal eigenvector is $\mathbf{v} = (1, -1, 0, \dots, 0)^\top$, whose associated eigenvalue is

$$\lambda = -Ck^{\eta+\mu} + k^{\nu+\rho}. \quad (3.35)$$

Using (3.33) we rewrite (3.35) in the form

$$\lambda = N^{Q_{\text{Neg}}} \left(1 - \frac{C}{N S_{\text{Neg}}} \right), \quad (3.36)$$

where now

$$Q_{\text{Neg}} = \beta(\nu + \rho) \quad (3.37)$$

$$S_{\text{Neg}} = \beta(\nu + \rho - \mu - \eta). \quad (3.38)$$

Hence under negative dynamics the stability classifier is different from (3.29), being $S_{\text{Neg}} = S - \beta$. For example, in Biochemical, where $\Omega = (-1, 1, -1, 0)$ we have $S_{\text{Neg}} = -\beta < 0$, predicting a stable dynamics.

4 Methods and data analysis

4.1 Numerical integration

To numerically test our predictions we constructed Eq. (1.1) for each of the systems in Sec. 2, using the appropriate A_{ij} (Scale-free, Erdős-Rényi, empirical, etc.). We then used a fourth-order Runge-Kutta stepper (Matlab's ode45) to numerically solve the resulting equations. Starting from an arbitrary initial condition $x_i(t=0)$, $i = 1, \dots, N$ we allowed the system to reach steady-state by waiting for $\dot{x}_i \rightarrow 0$. To numerically realize this limit we implemented the termination condition

$$\max_{i=1}^N \left| \frac{x_i(t_n) - x_i(t_{n-1})}{x_i(t_n) \Delta t_n} \right| < \varepsilon, \quad (4.1)$$

where t_n is the time stamp of the n th Runge-Kutta step and $\Delta t_n = t_n - t_{n-1}$. As the system approaches a steady-state, the activities $x_i(t_n)$ become almost independent of time, and the numerical derivative $\dot{x}_i = x_i(t_n) - x_i(t_{n-1})/\Delta t_n$ becomes small compared to $x_i(t_n)$. The condition (4.1) guarantees that the maximum of \dot{x}_i/x_i over all activities $x_i(t_n)$ is smaller than the pre-defined termination variable ε . In our simulations, across the different dynamics we tested, we set $\varepsilon \leq 10^{-12}$, a rather strict condition, to ensure that our system is sufficiently close to the *true* steady-state.

4.2 Numerically estimating J_{ij}

Once the steady state $\mathbf{x} = (x_1, \dots, x_N)^\top$ is reached we construct the *numerical* Jacobian by substituting the numerically obtained states x_i into (1.35) and (1.46). This represents the system's actual stability matrix, incorporating its specific dynamics on the relevant network A_{ij} . For example, consider our Social model in Eq. (2.3), where $M_0(x) = -fx$, $M_1(x) = 1 - x$ and $M_2(x) = gx$, and hence $M'_0(x) = -f$, $M'_1 = -1$ and $M'_2 = g$. Once we obtain \mathbf{x} we introduce all numerically calculated x_i into D_{ii} and W_{ij} , which for Social take the form

$$D_{ii} = -f + - \sum_{j=1}^N A_{ij} g x_j \quad (4.2)$$

and

$$W_{ij} = A_{ij}(1 - x_i)g. \quad (4.3)$$

In Fig. 2 of the main text we compare the scaling of these numerically estimated D_{ii} and W_{ij} vs. the theoretically predicted ensemble $\mathbb{E}(A_{ij}, \Omega)$, shown in (1.67) and (1.68).

4.3 Logarithmic binning

Our main theoretical prediction focuses on scaling relationships, such as $D(k) \sim k^\mu$, which we observe by their linear slope in a log-log plot. To construct such plots we employed logarithmic binning¹⁵. First we divide all nodes into B bins

$$\mathbb{B}(b) = \{i = 1, \dots, N \mid c^{b-1} < k_i \leq c^b\}, \quad (4.4)$$

where $b = 1, \dots, B$ and c is a constant. In (4.4) the b th bin includes all nodes i whose degrees k_i are between c^{b-1} and c^b . The parameter c is selected such that the unity of all bins $\cup_{b=1}^B \mathbb{B}(b)$ includes all nodes, hence we set $c^B = \max_{i=1}^N k_i$. We then plot the average degree of the nodes in each bin

$$k_b = \langle k_i \rangle_{i \in \mathbb{B}(b)} = \frac{1}{|\mathbb{B}(b)|} \sum_{i \in \mathbb{B}(b)} k_i \quad (4.5)$$

versus the average $D(k)$ term of nodes in that bin

$$D(k_b) = \langle D_{ii} \rangle_{i \in \mathbb{B}(b)} = \frac{1}{|\mathbb{B}(b)|} \sum_{i \in \mathbb{B}(b)} D_{ii}. \quad (4.6)$$

In a similar fashion we plot $W_{ij} \sim k_i^\nu k_j^\rho$, this time applying the binning on $k_i^\nu k_j^\rho$, instead of k_i . Therefore, the bins are defined as

$$\mathbb{B}(b) = \{(i, j) | A_{ij} = 1, c^{b-1} < k_i^\nu k_j^\rho \leq b^w\}, \quad (4.7)$$

such that in each bin we include all node pairs whose product $k_i^\nu k_j^\rho$ is within a given range. As above, we then plot the average W_{ij} in each bin, providing the real Jacobian terms

$$J_b^{\text{Real}} = \langle W_{ij} \rangle_{(i,j) \in \mathbb{B}(b)} = \frac{1}{|\mathbb{B}(b)|} \sum_{(i,j) \in \mathbb{B}(b)} W_{ij} \quad (4.8)$$

vs. the average value of $k_i^\nu k_j^\rho$ in that bin

$$J_b^{\text{Th}} = \langle k_i^\nu k_j^\rho \rangle_{(i,j) \in \mathbb{B}(b)} = \frac{1}{|\mathbb{B}(b)|} \sum_{(i,j) \in \mathbb{B}(b)} k_i^\nu k_j^\rho. \quad (4.9)$$

4.4 Model and empirical networks

To test our predictions we used model and real networks, as summarized below:

ER. An Erdős-Rényi random network with $N = 6,000$ nodes and an average degree of $\langle k \rangle = 6$.

SF1,2,3. A set of binary scale-free networks, constructed via the configuration model², with $N = 6,000$ nodes, $\langle k \rangle = 6$ and degree distribution following $P(k) \sim k^{-\gamma}$ with $\gamma = 2, 2.5$ and 3 , respectively.

UCIonline (Social). An instant messaging network from the University of California Irvine¹⁶, capturing 61,040 transactions between 1,893 users during a $T = 218$ day period. Connecting all individuals who exchanged messages throughout the period, we obtain a network of 1,893 nodes with 27,670 links, exhibiting a fat-tailed degree distribution.

Email Epoch (Social). This dataset monitors $\sim 3 \times 10^5$ emails exchanged between 3,185 individuals over the course of ~ 6 months¹⁷, giving rise to a scale-free social network with 31,885 binary links.

PPI1 (Regulatory, Biochemical). The yeast scale-free protein-protein interaction network, consisting of 1,647 nodes (proteins) and 5,036 undirected links, representing chemical interactions between proteins¹⁸.

PPI2 (Regulatory, Biochemical). The human protein-protein interaction network, a scale-free network, consisting of $N = 2,035$ nodes (protein) and $L = 13,806$ protein-protein interaction links¹⁹.

ECO1,2 (Ecological). To construct the mutualistic ecological networks we collected data on symbiotic interactions of plants and pollinators in Carlinville Illinois from²⁰. The resulting $456 \times 1,429$ network M_{ik} is a bipartite graph linking the 456 plants with their 1,429 pollinators. When a pair of plants is visited by the same pollinator they mutually benefit each other indirectly, by increasing the pollinator populations. Similarly pollinators sharing the same plants also posses

an indirect mutualistic interaction. Hence we can collapse M_{ik} to construct two mutualistic networks: The 1,429 × 1,429 pollinator network ECO1 and the 456 × 456 plant network ECO2. The resulting networks are

$$B_{kl} = \sum_{i=1}^{456} \frac{M_{ik}M_{il}}{\sum_{s=1}^n M_{is}}, \quad (4.10)$$

for the pollinator network (ECO1), and

$$A_{ij} = \sum_{k=1}^{1,429} \frac{M_{ik}M_{jk}}{\sum_{s=1}^n M_{sk}}, \quad (4.11)$$

for the plant network (ECO2). In both networks the numerator equals to the number of mutual plants (B_{kl}) or pollinators (A_{ij}). For each mutual plant i (pollinator k) we divide by the overall number of plants (pollinators) that share i (k). Hence, the weight of the mutualistic interaction in, *e.g.*, A_{ij} is determined by the density of mutual symbiotic relationships between all plants, where: (i) the more mutual pollinators k that plants i and j share the stronger the mutualistic interaction between them; (ii) on the other hand the more plants pollinated by k the smaller is its contribution to each plant. A similar logic applies also for the pollinator network B_{ij} . This process potentially allows us to have isolated components, *e.g.*, single disconnected nodes. The state of these isolated nodes is decoupled from the state of the rest of the network, and hence in our analysis we only focused on the giant connected component of A_{ij} and B_{ij} , comprising all 456 plants, rendering A_{ij} to be a fully connected component, but only 1,044 pollinators, eliminating 385 isolated pollinators in B_{ij} .

5 Mixed dynamics

Our analytical derivation revolves around cooperative interactions, in which $A_{ij} \in \{0, 1\}$, *i.e.* non-negative, and the functions $M_1(x), M_2(x)$ in (1.1) are also positive for all x . The only exception is our Biochemical model, in which the hetero-dimer interaction ($-A_{ij}x_i x_j$) captures depletion of i and j , and hence all interactions are negative. Some applications, however, involve a mixture of cooperative and adversarial interactions, requiring us to analyze signed networks in which $A_{ij} \in \{-1, 0, 1\}$. A classic example is in population dynamics, which, in many cases, represent a mixture of mutualistic interactions, coexisting alongside competitive and predatory dynamics. Strictly speaking, under these conditions, the Jacobian J_{ij} cannot be extracted from the $\mathbb{E}(A_{ij}, \Omega)$ ensemble. Yet, as we next show, even then, our theory can still help us understand the emergence of stability.

Consider the Ecological model

$$\frac{dx_i}{dt} = Bx_i(t) \left(1 - \frac{x_i(t)}{K}\right) + \sum_{j=1}^N A_{ij}x_i(t) \frac{x_j}{1 + x_j}, \quad (5.1)$$

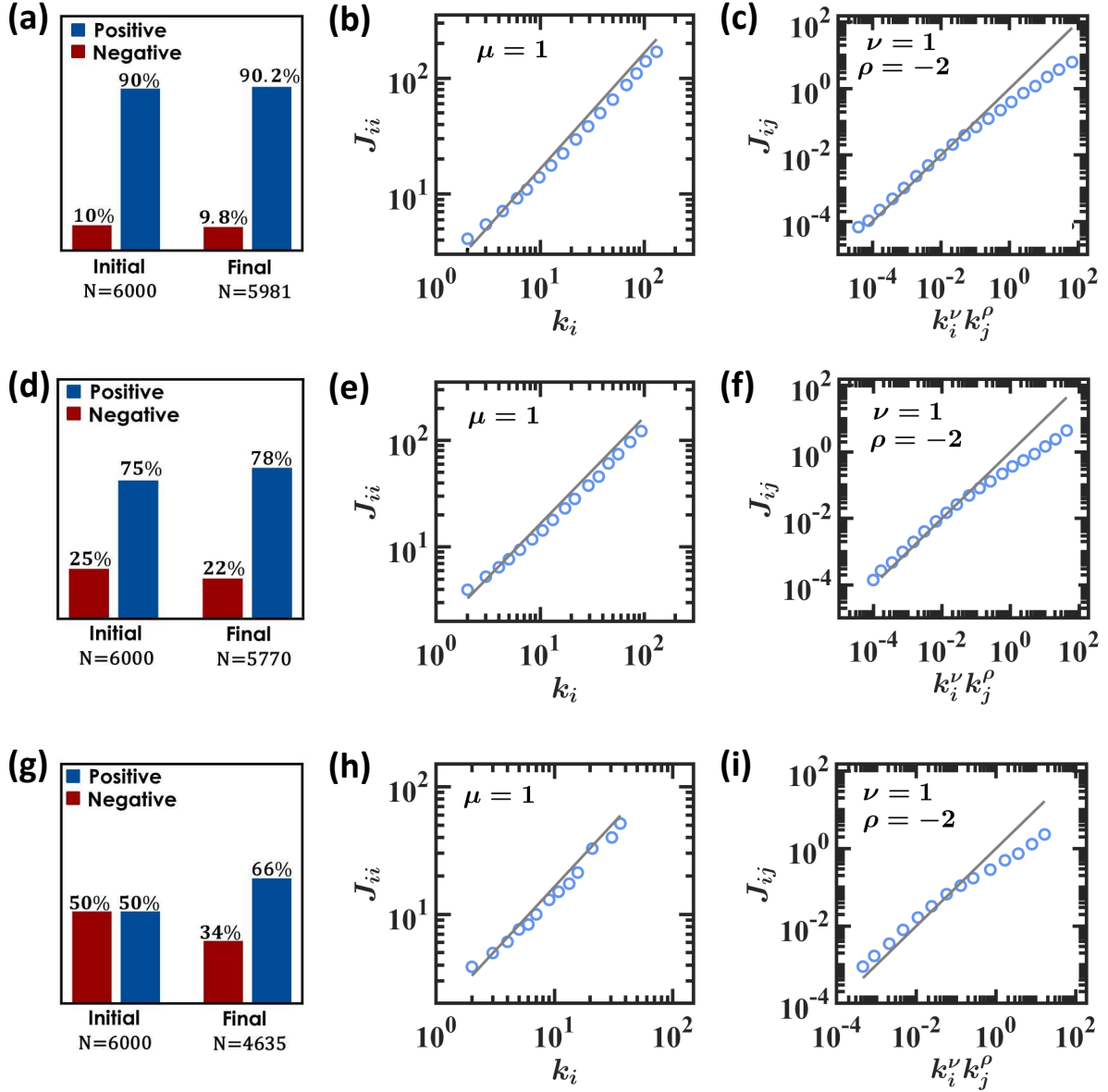


Figure 8: **Emerging stability under mixed interactions.** (a) Starting with a scale-free A_{ij} with 10% negative links, the system reaches a fixed-point in which nodes with many negative links become extinct. As a result the surviving 5,981 node-network is slightly biased towards positive links (9.8% vs. the initial 10% negative). (b) The Jacobian matrix continues to follow the analytically predicted scaling $J_{ii} \sim k_i^\mu$, selectively for the (majority) of positive k_i . (c) Similarly the off-diagonal terms also follow the predicted $J_{ij} \sim k_i^\nu k_j^\rho$ (for $k_i, k_j > 0$). (d)-(f) Similar analysis for an initial 25% negative links. (g)-(i) Even under 50% negative links the surviving network Jacobian (4,635 nodes) can still be approximated by $\mathbb{E}(A_{ij}, \Omega)$.

in which the existing links in A_{ij} include a random fraction of $0 \leq f \leq 1$ negative interactions ($A_{ij} = -1$) and a remaining $1 - f$ fraction of links that are positive ($A_{ij} = 1$). As the system evolves in time, the activities $x_i(t)$ are positively impacted by the cooperative interactions, but suppressed by the adversarial ones. Therefore, nodes with many negatively interacting partners will have their activities driven towards $x_i(t) \rightarrow 0$. The crucial point is that once a node reaches zero activity, it becomes extinct, and effectively removed from the network, together with its set of links. As a consequence the system will reach a steady state, in which the surviving nodes are biased towards positive k_i . *This represents a quite general, and most importantly, a naturally emerging organizing principle that leads real world A_{ij} to have a majority positive set of links.*

To exemplify this, we constructed a scale free A_{ij} with $N = 6,000$ nodes and $L = 18,000$ links, of which a fraction $f = 0.1$ are negative, representing a 10% adversarial network. Starting from an arbitrary initial condition, we allowed the system (5.1) to naturally reach its fixed-point. During the process, whenever a specific activity reached $x_i(t) \leq \epsilon$ we set it permanently to zero (extinction), effectively removing it from the network; we used $\epsilon = 10^{-12}$. At its final state the network is reduced to $N = 5,981$ surviving nodes, featuring a (slight) decrease in the fraction of negative links, from 10% to 9.8% (Fig. 8a). This is a minor effect, of course, however, as we increase the negative link fraction, f , this positive-link bias becomes more pronounced. Indeed, under an initial condition where $f = 0.25$, the system reached a final state in which the negative links are reduced to 22% (Fig. 8d), and, finally, starting with a balanced positive-negative network ($f = 0.5$), we find, after pruning the extinct nodes, that the final surviving network is 66% positive (Fig. 8g).

For each of these three network, once reaching a fixed point, we extracted numerically their Jacobian matrix, as explained in Sec. 4.2. As expected, the resulting J matrices include both positive and negative weights, and hence, strictly speaking $J \notin \mathbb{E}(A_{ij}, \Omega)$. However, thanks to the pruning effect, the actual J matrices remain predominantly positive, and the majority of surviving nodes continue to have $k_i > 0$. Hence, while imperfect, we still observe that J follows (approximately) the scaling patterns of the $\mathbb{E}(A_{ij}, \Omega)$ ensemble. Indeed, Fig. 8b,c,e,f,h,i confirms that, despite the inclusion of negative links, J_{ii} and J_{ij} continue to follow (1.67) and (1.68) with $\mu = 1, \nu = 1$ and $\rho = -2$, as predicted for Ecological.

Taken together, this exemplifies that both under fully positive and under mixed interactions, real-world Jacobian matrices are, indeed, non-random, exhibiting (exactly or approximately) the unique interplay between topology and dynamics expressed in $\mathbb{E}(A_{ij}, \Omega)$. These patterns require no *devious strategies*, but rather arise from naturally emerging organizing principles: for positive dynamics - the scaling Ω , and for mixed interactions that, in combination with the pruning of negative links via extinction.

References

- [1] B. Barzel and A.-L. Barabási. Universality in network dynamics. *Nature Physics*, 9:673 – 681, 2013.
- [2] M.E.J. Newman. *Networks - an introduction*. Oxford University Press, New York, 2010.
- [3] J. Gao, B. Barzel and A.-L. Barabási. Universal resilience patterns in complex networks. *Nature*, 530:307–312, 2016.
- [4] G. Caldarelli. *Scale-free networks: complex webs in nature and technology*. Oxford University Press, New York, 2007.
- [5] S. Boccaletti, V. Latora, Y. Moreno, M. Chavez and D.-U. Hwang. Complex networks: Structure and dynamics. *Physics Reports*, 424:175–308, 2006.
- [6] L. Schmetterer and K. Sigmund (Eds.). *Hans Hahn Gesammelte Abhandlungen Band 1/Hans Hahn Collected Works Volume 1*. Springer, Vienna, Austria, 1995.
- [7] R.M. May. Will a large complex system be stable? *Nature*, 238:413 – 414, 1972.
- [8] P.S. Dodds and D.J. Watts. A generalized model of social and biological contagion. *Journal of Theoretical Biology*, 232:587–604, 2005.
- [9] G. Karlebach and R. Shamir. Modelling and analysis of gene regulatory networks. *Nature Reviews*, 9:770–780, 2008.
- [10] B. Barzel and O. Biham. Binomial moment equations for stochastic reaction systems. *Phys. Rev. Lett.*, 106:150602–5, 2011.
- [11] R.M. May. Simple mathematical models with very complicated dynamics. *Nature*, 261: 459–467, 1976.
- [12] C.S. Holling. Some characteristics of simple types of predation and parasitism. *The Canadian Entomologist*, 91:385–398, 1959.
- [13] E.O. Voit. *Computational Analysis of Biochemical Systems*. Cambridge University Press, New York, NY, 2000.
- [14] H.I. Schreier, Y. Soen and N. Brenner. Exploratory adaptation in large random networks. *Nature Communications*, 8:14826, 2017.
- [15] S. Milojević. Power-law distributions in information science: making the case for logarithmic binning. *Journal of the American Society for Information Science and Technology*, 61:2417–2425, 2010.
- [16] T. Opsahl and P. Panzarasa. Clustering in weighted networks. *Social Networks*, 31:155–163, 2009.
- [17] J.-P. Eckmann, E. Moses and D. Sergi. Entropy of dialogues creates coherent structures in e-mail traffic. *Proc. Natl. Acad. Sci. USA*, 101:14333–7, 2004.
- [18] H. Yu *et al.* High-quality binary protein interaction map of the yeast interactome network. *Science*, 322:104–110, 2008.

- [19] J.F. Rual *et al.* Towards a proteome-scale map of the human protein-protein interaction network. *Nature*, 437:1173–1178, 2005.
- [20] Interaction web database. <http://www.nceas.ucsb.edu/interactionweb/resources>.